NASA CONTRACTOR REPORT

N.A.S.A. CR-627

AN EXPERIMENTAL STUDY OF FLUIDIZATION PROCESSES UNDER LUNAR CONDITIONS

by Gordon H. Miller and Irving R. King

Prepared by
TEXACO EXPERIMENT, INC.
Richmond, Va.
for Goddard Space Flight Center

NATIONAL AERONAUTICS AND SPACE ADMINISTRATION • WASHINGTON, D. C. • OCTOBER 1966

AN EXPERIMENTAL STUDY OF FLUIDIZATION PROCESSES UNDER LUNAR CONDITIONS

By Gordon H. Miller and Irving R. King

Prepared under Contract No. NAS 5-9231 by
TEXACO EXPERIMENT, INC.
Richmond, Va.

for Goddard Space Flight Center

NATIONAL AERONAUTICS AND SPACE ADMINISTRATION

For sale by the Clearinghouse for Federal Scientific and Technical Information
Springfield, Virginia 22151 – Price $2.50

TABLE OF CONTENTS

LIST OF TABLES

LIST OF ILLUSTRATIONS

ABSTRACT

Fluidized ash flow has been proposed in the literature (5 and 6) as the volcanic means by which the lunar maria have been formed. If this process could be reasonably established as the origin of the maria, then the Ranger and Surveyor program information could be more effectively interpreted and a better foreknowledge of lunar landing conditions could be obtained. The program reported herein was undertaken to examine, in the laboratory, certain factors of fluidization which could lead to a relatively large-scale demonstration of fluidized ash flow. The program object was to select the best material for simulating lunar soils for such a demonstration and to ascertain the effect on fluidization of the hard vacuum of the lunar environment.

Talc, spent fluidized catalyst, high-porosity fluidized catalyst, granite dust, ash-flow tuff and glass microspheres were examined in laboratory fluidization equipment to determine: a) the effect of size, size distribution, and shape on settling rate after fluidization vapor is cut off; b) the maximum size which will permit satisfactory horizontal flow; and c) such physical data as voids fraction, surface area, density and bulk density of the materials. An examination was also made of the effect of vacuum on fluidization in the pressure region below about 4 torr where the mean free path of the gas is of the order of the particle size to determine: a) if fluidization is affected, b) the probable depth below the surface where fluidization is altered, c) the maximum gas flows allowable without violent bubbling and d) the effect on bed expansion and pressure drop through the bed.

It was concluded that the fluidization properties of various materials could be rated so that the best material for a large scale demonstration of fluidized ash flow could be made in the laboratory. The best material, judged by flowing the greatest distance, having the highest travel velocity and the slowest settling rate is the F-2-25 catalyst. This material will require no separation or grinding before use. The effects of particle size and size distribution on fluidization were important and these are described in detail. The distance particles will flow correlates well with the factor of expansion ratio divided by particle density and settling rate.

It was established that low pressure, in the range where the mean free path of the vapor becomes larger than the particle dimensions, has a pronounced effect on fluidization. The maximum gas flow through the bed without violent bubbling is at least an order of magnitude less under these vacuum conditions

than for fluidization at one atmosphere. The hypothetical distance below the surface where fluidization can still occur in a vacuum is between about 4 to 8 cm for FCCU catalyst which was the easiest material to fluidize. Bed expansion ratio is decreased as the pressure is lowered near the critical point and approaches unity (no expansion) rapidly below 1 torr. The ratio also is decreased as the bed height is increased and at 1 torr it approaches unity between 40-50 cm of bed height. From all this, it is seen that in a fluidized system of major dimensions, the effect of vacuum is to cause the top surface to erupt into a dilute phase and to cause extensive elutriation. This dilute phase then falls back to the surface at the end of the eruption.

It is recommended that F-2-25 catalyst be used for a large scale demonstration of fluidized ash flow and that recognition be given to the effect that vacuum has had on the mechanism of a lunar ash flow. This means that in addition to possible dense phase flow, similar to terrestrial ash flows, lunar flows must have been accompanied by an extensive dilute phase sent upward and falling back to the surface near and immediately following the end of the eruption.

Future problems which merit study, in addition to a large scale demonstration, concern the effect of the dilute phase falling back to the moon and the nature of the resultant surface which is formed. A suggested experimental program is briefly outlined.

I. INTRODUCTION

A major goal of the National Aeronautics and Space Administration is a manned landing on the moon. One key question that requires answering before this attempt is made is how the landing will be affected by the nature and condition of the lunar surface. Until recently, the most definitive knowledge of the lunar surface has come from the studies of the photometric curves of reflected sunlight and of radar-reflection data. These have given some ideas of the nature of the very outer surface in the centimeter and meter range. At slightly lower depths, which are regions of concern for the physical support of the manned landing spacecraft, the situation is less clear. In the maria, where landing is planned, it is not known whether the composition is powdery or hard, loosely compacted or dense. Instrument explorations via the Ranger and Surveyor programs have been expected to eventually answer these questions. However, the Ranger pictures, while interpreted by many as indicating a satisfactory landing surface, are believed by some to show deep dust and an unsatisfactory surface. The pictures alone have not settled the controversy. The more recent Russian soft landing in the Sea of Storms has indicated, at least for that region, that a 100 kilogram sphere could be landed satisfactorily. It has not yet been established if deep dust was present or not. The Surveyor will, hopefully, establish the surface conditions, but to fully interpret the results, it will be of immense aid if a better understanding exists as to how the maria were formed.

Maria formation and conditions are described by a number of conflicting theories. These include formation by the flow of molten lava (Baldwin (1)), the melting of planetesimals (Urey (2)), and deep dust that was transported from the highlands (Gold, (3)). All of these theories have certain drawbacks. A more recent theory involves maria formation by the flow of fluidized ash. This concept has been tentatively indicated by Shoemaker and Hackman (4) and discussed in considerable detail by O'Keefe and Cameron (5), and by O'Keefe and Adams (6).

Fluidized-ash flow appears to much better explain the lunar features of the maria than any of the others. If this process can be reasonably established as the origin of the maria, then it will stand as a theory to be tested by the Surveyor program. Data obtained from these explorations can be more intelligently interpreted as a result, and foreknowledge of lunar landing conditions will thereby be enhanced.

The current program was undertaken to examine, in the laboratory, certain aspects of fluidization which could lead to a relatively large-scale demonstration of the flow of fluidized ash. In particular, it seeks to select those materials most suitable for simulating lunar soils in a fluidization experiment and to deduce the effect that the lunar hard vacuum will have on the fluidization process.

A. MARIA FORMATION BY FLUIDIZED ASH FLOW

An excellent statement of the fluidized-ash-flow concept on the moon is given by O'Keefe and Cameron (5), who point out the similarities between the lunar surface and the comparatively recently recognized mechanism of the flow of volcanic ash on earth. The latter has been extensively reviewed by Ross and Smith (7).

1. Flow of Terrestrial Ash

An ash flow is described by Ross and Smith as a "turbulent mixture of gas and pyroclastic materials of high temperature, ejected explosively from a crater or fissure, that travels swiftly down the slopes of a volcano or along the ground surface. The solid material in an ash flow, although unsorted, is dominantly of particles of ash size (less than 4 mm in diameter) but generally contains different amounts of lapilli and blocks." The deposit from an ash flow may be consolidated and is then known as an ash-flow tuff, or it may be welded and is then called a welded tuff.

Some of the early recognition of sand or ash flow was the volcanic action that occurred in the Katmai region of Alaska which gave rise to the "Valley of 10,000 Smokes". Fenner (8) stresses the "remarkable character imparted to the dust and gas mixture by the continuous evolution of gas which must not only have eliminated almost completely the contact friction of the particles but also have tended to drive them apart somewhat forcibly and caused the mass to spread almost as freely as a true liquid." Griggs (9), describing the same Katmai region, commented that "surrounded as it is by high rugged mountains, the most striking feature of the conformation of the Valley of 10,000 Smokes is the flatness of its floor. One could ride a bicycle for miles along its smooth surface. Altogether it occupies an area of 53 square miles (137 sq km)."

Single ash flows may be quite extensive, covering areas up to 10,000 square miles at depths from 60 to 500 ft (150 meters). The flow around Lake Tobe,

Sumatra, is comprised of 2000 cubic kilometers of erupted matter (10). Dolgoff (11) traced individual sheets in the Pahranaget area of Nevada for 100 miles.

The speed of flow may be high, in the range of 60 to 100 miles per hour (7, pg 41). At the edges, the flow conforms to the containing walls like liquid at a shore line. Ash flow temperatures have been determined by Boyd (12) to be about 850°C. Heat is retained for long periods of time, and welding may take place, particularly in the middle. The top (and frequently the bottom) where heat escapes more readily, is less likely to be welded. The settling or collapse of the original porous structure is greatest where the ash is deepest, and, as Boyd has indicated, the surface will often tend to show the features of the covered surface below, although they would be diminished in height and depth.

2. Flow of Lunar Ash

In view of the above, the formation of lunar maria by the flow of fluidized ash seems to be a good possibility. Many features or observations of the moon are explainable by this mode, or at least are not in conflict with it.

a. Absence of Scarps. Scarps that are typical of molten lava are not seen. Fluidized-ash laydown would not show sudden breaks at the terminus of flow.

b. Absence of Blocky Substrate. Radar data show smoothness of the order of meters or more deep, and basaltic flow would be expected to be blocky on this scale. Fluidized-ash laydown is consistent with radar results.

c. Ghost Craters. Ghost craters such as those seen, for example, in Mare Nectaris and Mare Humorum, are best explained by the flow of fluidized ash. Pre-maria craters are believed to have been covered by the ash flow and their forms revealed by the settling and compaction of the ash.

d. Color of Maria. The relatively uniform color of individual mare is consistent with the uniform spread of fluidized material (uniform composition is observed in terrestrial flows). Since the color appears to be of shallow depth, it is suggested by us (but with no present experimental evidence) that the color near the surface may have been caused by chemical reactions of escaping volatiles that were associated with the fluidizing steam. In this connection, Urey (private communication) has pointed out the interesting five

or so dark spots that are visible on the floor of Alphonsus crater, where volcanic gases (identified as containing C_2) were observed by Kozyrov (13). Radiation darkening of the surface of ash-flow deposit should also be considered a possibility.

e. Comparative Age of Maria. The maria were apparently formed at about the same time, as indicated by Shoemaker's and Hackman's counts (14) of post-mare craters in all the major lunar dark areas. The random craters showed the same frequency pattern in all areas (with the possible exception of Mare Crisium). The flow of fluidized ash from volcanic events could probably take place over a comparatively short span of time.

f. Heat Balance. Ash flow would require less heat than lava flow, and this may be an important consideration in any re-examination of lunar heat balance.

g. Feasibility of Fluidized Ash Flow. O'Keefe and Cameron (5) have very clearly shown that lunar conditions of reduced gravity actually favor deposition of more extensive tuff from ash flow on the moon than under terrestrial conditions. Because of lower gravitational pull, the weight of the material to be supported is less, and the pressure and specific gravity are less at every depth. This means that less fluidizing gas is required, resulting in a factor of about 33 in favor of ash flow on the moon.

B. EXPERIMENTAL STUDY AND DEMONSTRATION OF SIMULATED FLOW OF FLUIDIZED ASH

The flow of fluidized ash appears plausible as a phenomenon for formation of maria, but it is believed that a convincing demonstration, and an experimental establishment of certain facts, would lead to a more widespread acceptance of such a mechanism. For this reason the current program was undertaken.

1. Description of the Fluidization Process

Fluidization of particles is a well-known industrial technique used in such instances as fluid transport of powders, dusts, and cereal grains. When vapor is passed through a bed of particles in a tube at a velocity that is sufficiently high, a condition known as incipient fluidization results. This occurs when the pressure-drop across the bed equals the weight of the bed divided by the area. With a slight increase in velocity, the bed begins to expand, and the particles tend to separate from each other and to rest on a cushion of vapor. This reduces the interparticle friction substantially, and the resulting

bed of particles behaves as a fluid and has a characteristic viscosity. This fluidized bed will "float" denser objects and will have flow characteristics that are very similar to a liquid. Over a certain range of velocity, the bed and vapor will reach a more or less steady-state condition, and the viscosity of the fluidized bed will remain relatively constant.

At higher velocities, however, severe bubbling and slugging will take place, and at still higher velocities, the bed will be lifted out of the tube.

Many variables affect the fluidization phenomena. These include the density, size, size distribution, and shape of the particles; density, viscosity, and velocity of the fluid; the total pressure; and the gravitational field. The effects of many of the above factors are fairly well established for industrial processes but they need to be re-examined in the unusual environment of the moon.

2. Problems in Demonstrating Ash Flow

For a flow on the moon which may be 100 meters or more deep, the fluidizing steam will undergo a substantial expansion and will increase in velocity as it rises toward the top. This driving force (of pressure drop and vapor flow through the ash) is on such a large scale in nature that it is difficult to simulate in a demonstration. Furthermore, the water is diffusing from the interior of the particles and being continually emitted as steam for a substantial period of time or may cause a vesiculation or a "popcorn" explosion of many of the particles. It is a simple matter to show fluid properties of a column of particles in a container with fluidizing vapor being continuously passed upward through it. However, to demonstrate any extended horizontal travel of an ash flow, which must contain its own fluidizing vapor and possess the requisite liquid-like properties, is somewhat difficult.

3. Possible Demonstration of Ash Flow

It occurred to us, however, that based on experience with a unique operation called the Texaco Fine Grinding Process, a demonstration might be possible. It was observed that if hot and very finely ground talc was accidentally spilled from the equipment, it flowed across the floor like a liquid.

In the Texaco process, after the material has been finely ground, it is transported in super-heated steam to a cyclone, where excess steam is removed and the hot powder, still containing some dry superheated steam, is sent to a storage vessel or silo. There, because of the excellent thermal insulation

properties of the powder, it remains very hot for long periods of time. This material could be used for a very effective demonstration of the flow of fluidized ash.

4. Composition of Material for Fluidized Flow

Rather than talc, it would be preferred if the simulated ash flow could be made with the same rock particle composition as occurs on the moon. Unfortunately, this composition is not known, so it can only be assumed. O'Keefe and Cameron (5) have discussed the possibility of lunar granites and have given support to the theory that tektites may come from the moon. The tektites are similar in a number of respects to earth granites but contain more quartz and, presumably, have lost K_2O and Na_2O by some process. It is possible that this may have resulted from elutriation fractionation during ash-flow processes on the moon. However, for the time being, granites or their volcanic equivalents, rhyolites, appear to be among the better simulations to use. Actually, an ash-flow tuff from California, New Mexico, or Nevada would be an excellent choice.

The Texaco fine-grinding equipment has handled such substances as talc, kaolin, barites, limestone, coal, and feldspar (the latter is a granite component). Therefore, it could handle any desired rock. However, the fineness of product is related to the size of crushed and powdered material charged to it. It would save considerable expense if fairly fine charge material were already available. Talc and spent fluidized catalyst (sodium aluminum silicate) are available. It would be important, too, to know the maximum size of particles which will permit satisfactory horizontal flow so as to minimize fine grinding and more nearly simulate the sizes found in nature. Furthermore, a technical problem exists. It is known that the finely ground talc can be used satisfactorily for the demonstration as far as the fluidized flow is concerned, but it is not completely certain that some other minerals will do as well. Talc is in the form of small, flat platelets and, therefore, differs in its particle action from granites, for example, which are apt to be rough granules.

In view of the above, it was proposed to make small-scale fluidization studies of several materials, including talc, spent fluidized catalyst, high-porosity fluidized catalyst, granite, and an ash-flow tuff to determine which shall be used for the large-scale demonstration. Glass microspheres were included to serve as a reference. The data from this study will permit selection of the material to use for the large demonstration after consultation with the NASA project scientists.

5. Effect of Vacuum on Fluidization

One of the chief technical questions that is raised when lunar fluidized-ash flows are considered is the effect of vacuum on the process. A sound argument can be made that the effect is essentially trivial for deep ash flows. The equation relating to the minimum flow of gas necessary to fluidize a bed actually derives from Poiseuille's equations for capillary flow. However, this equation breaks down at very low pressures, where the mean free path of the gas approaches the dimensions of the particles, and viscous forces no longer act to support the particles. However, calculations by O'Keefe (private communication) indicate that the depth at which viscous forces begin to support the particles to be in the order of 5 cm or so below the surface. Therefore, in flows 100 meters deep, this will have insignificant overall effect. However, the top portion, no longer fluidized, would be expected to be blown upward by the rapidly expanding gases and form a dilute phase or cloud similar to the nuée ardente of the Mont Pelée eruption (15).

C. OBJECT AND SCOPE OF PROGRAM

The overall object of the program reported herein was to examine, in the laboratory, certain aspects of fluidization which could lead to a relatively large-scale demonstration of fluidized-ash flow such as may form the lunar maria. The specific objects were to select those materials most suitable for simulating lunar soils in a fluidization experiment and to deduce the effect that the lunar hard vacuum will have on the fluidization process.

The scope of the program involves:

1.) The examination, on small laboratory fluidization equipment, of several materials including talc, spent fluidized catalyst, high-porosity fluidized catalyst, granite, ash-flow tuff and glass microspheres to determine:

   a) Effect of size, size distribution, and shape on settling rate after fluidization vapor is cut off.

   b) Maximum size which will permit satisfactory horizontal flow.

   c) Physical data such as voids fraction, surface area, density, and bulk density.

2.) The examination of the effect of vacuum on fluidization in the pressure region where the mean free path of the gas is of the order of the particle size to determine:

a) If fluidization is affected,

b) The probable depth below the surface where the fluidization is altered,

c) Maximum gas flows allowable without violent bubbling, and

d) The effect on bed expansion and pressure drop through the bed.

D. ACKNOWLEDGEMENTS

The authors wish to acknowledge the effective laboratory work carried out by Mr. Leigh R. Middleton, Research Technician, who performed the particle sizing and both the atmospheric pressure and vacuum fluidization experiments. Our thanks is given to Barbara G. Fox and Thomas W. Langley for microphotographs of particles and to Bernard D. Von Cannon and Thomas E. Kagels for photographs of the fluidized-flow experiments.

II. EXPERIMENTAL WORK

A. MATERIALS USED IN FLUIDIZATION STUDIES

1. Particle Shapes

Materials for fluidization studies were chosen to represent a variety of shapes, porosities, and possible simulations of lunar soils. The nonporous materials were: glass microspheres (spherical) shown in Fig. 1, talc (flat particles) shown in Fig. 2, and granite dust (rough blocky) shown in Fig. 3. Porous materials were: fluid catalytic cracking unit (FCCU) catalyst (medium porosity - generally spherical) shown in Fig. 4, F-2-25 catalyst (high porosity - smooth irregular shape) shown in Fig. 5, and fluidized-ash-flow tuff (low porosity - rough shape) shown in Fig. 6. This latter picture shows the shape of the small particles (below 44 microns) of fluidized-ash flow, and the general shapes are retained in the larger particles as well. Figure 7 shows representative particles larger than 6.35 mm (1/4 in.). These are smoothly rounded but generally vesiculated. Figure 8 shows particles in the 590 to 840 micron range. In this size, it is possible to see several types of particles and, as will be of interest in a later section, it was found that the particle densities also varied. The appearance and density are tabulated as follows:

Photo appearance	Particle appearance	Particle Density, g/cm^3
Black	Black, nonporous	2.37
	Dark brown, nonporous	2.40
White	Translucent or clear, nonporous	2.55
Gray	White, porous or vesiculated	1.43

2. Source of Materials.

The source of the materials is shown in Table I.

3. Particle Size and Distribution

The materials as received were analyzed for particle size distribution by standard sieve techniques. The screening was done by using a rotary tapping

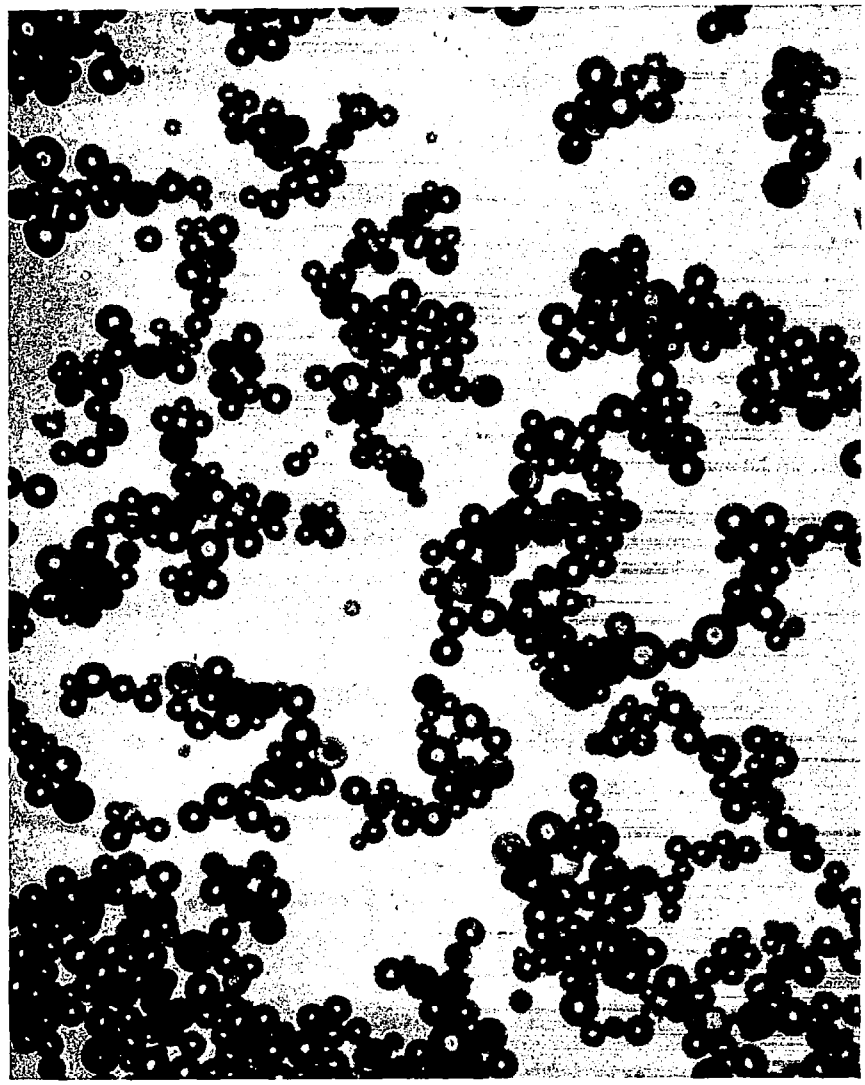

TEI-859

Fig. 1 Glass Microspheres No. 4000 (Approx. 20 to 40 Microns)

Fig. 2 Talc No. 325 (Smaller Than 44 Microns)

TEI-861

Fig. 3 Granite Dust (63 to 74 Microns)

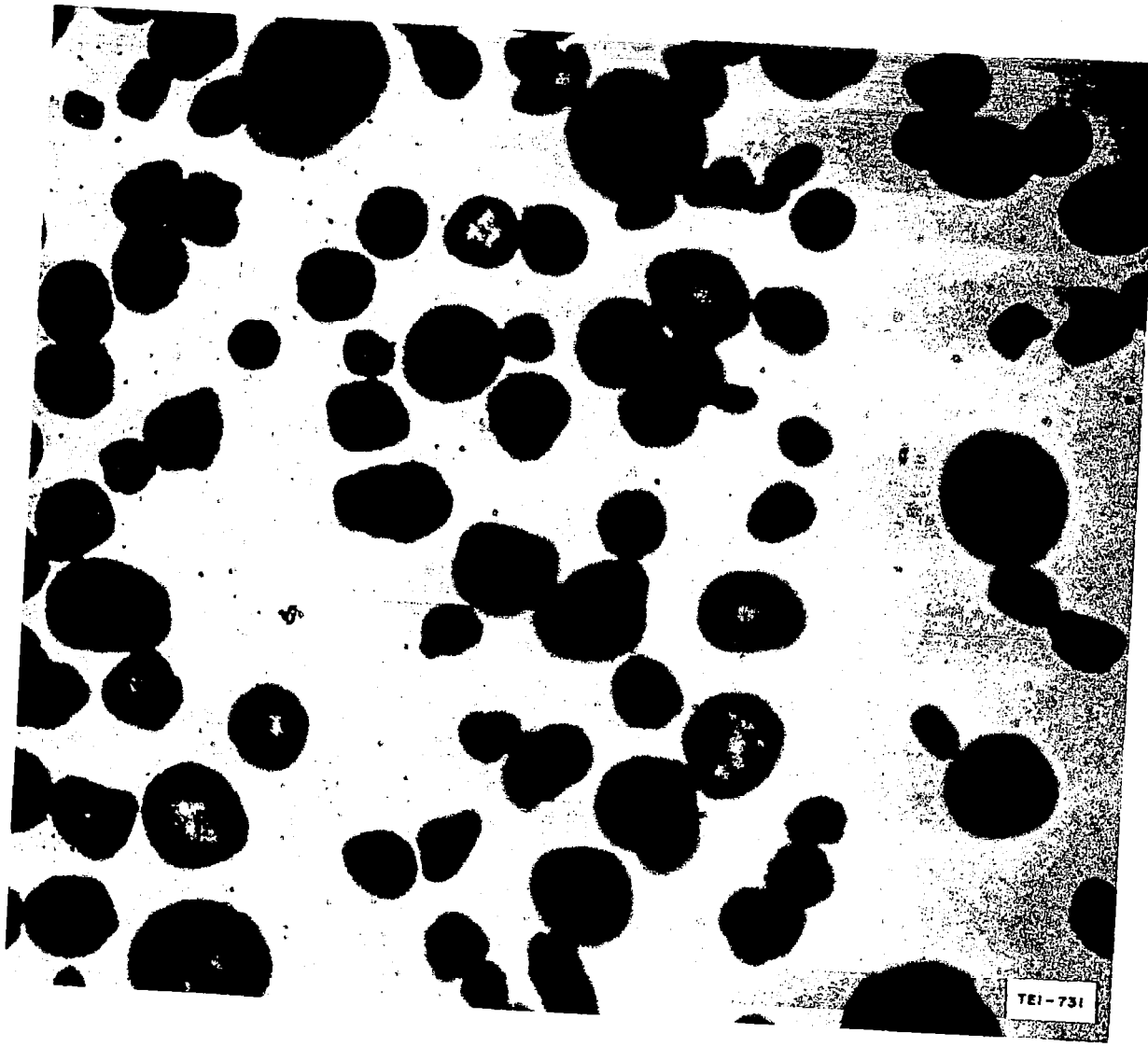

Fig. 4 Fluid Catalytic Cracking Unit (FCCU) Catalyst, Unsized (Smaller Than 105 Microns)

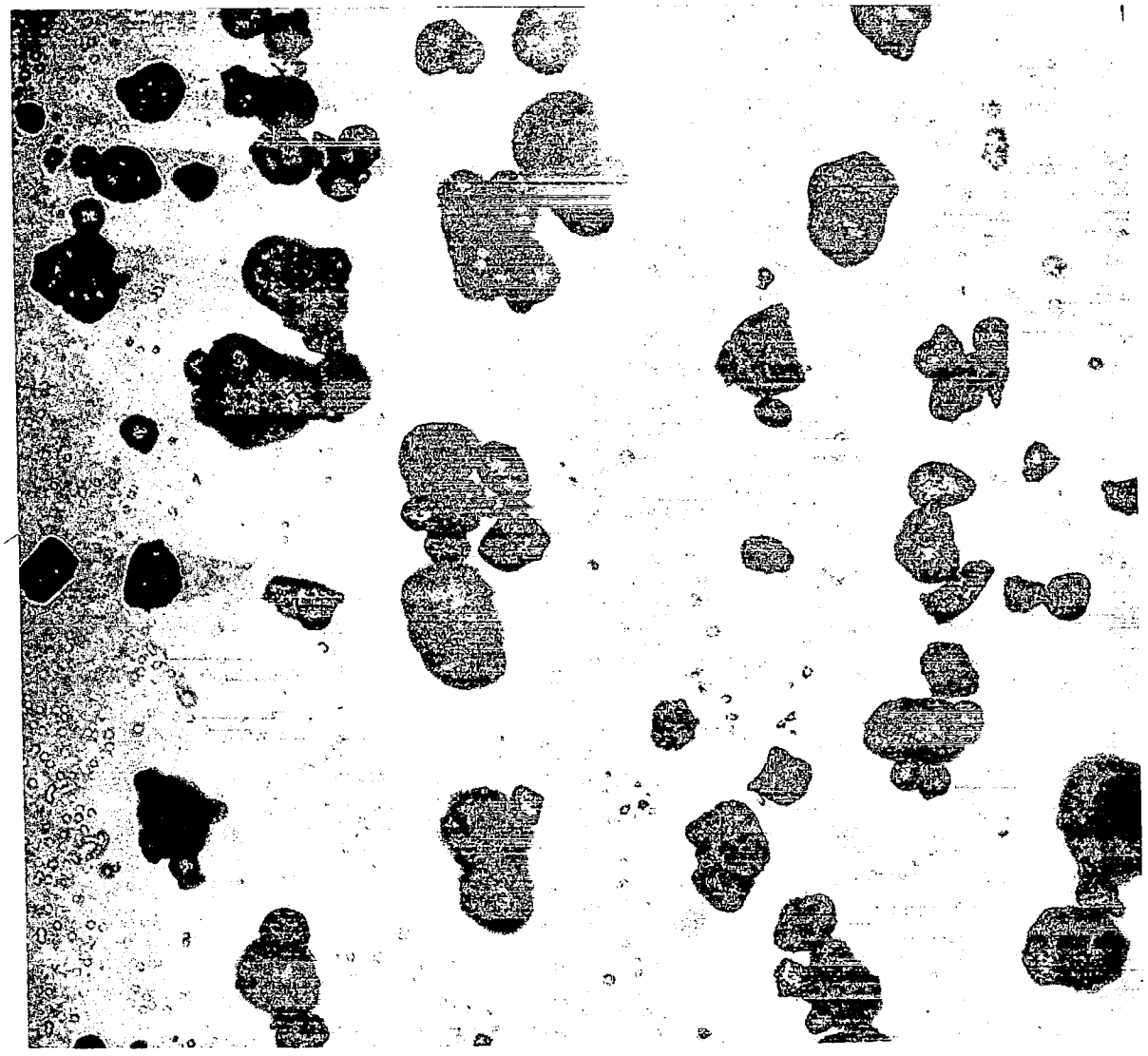

Fig. 5 F-2-25 Catalyst, Unsized (20 to 105 Microns)

Fig. 6 Fluidized Ash Flow Tuff (Smaller Than 44 Microns)

Fig. 7 Fluidized Ash Flow Tuff (Larger Than 6.35 mm)

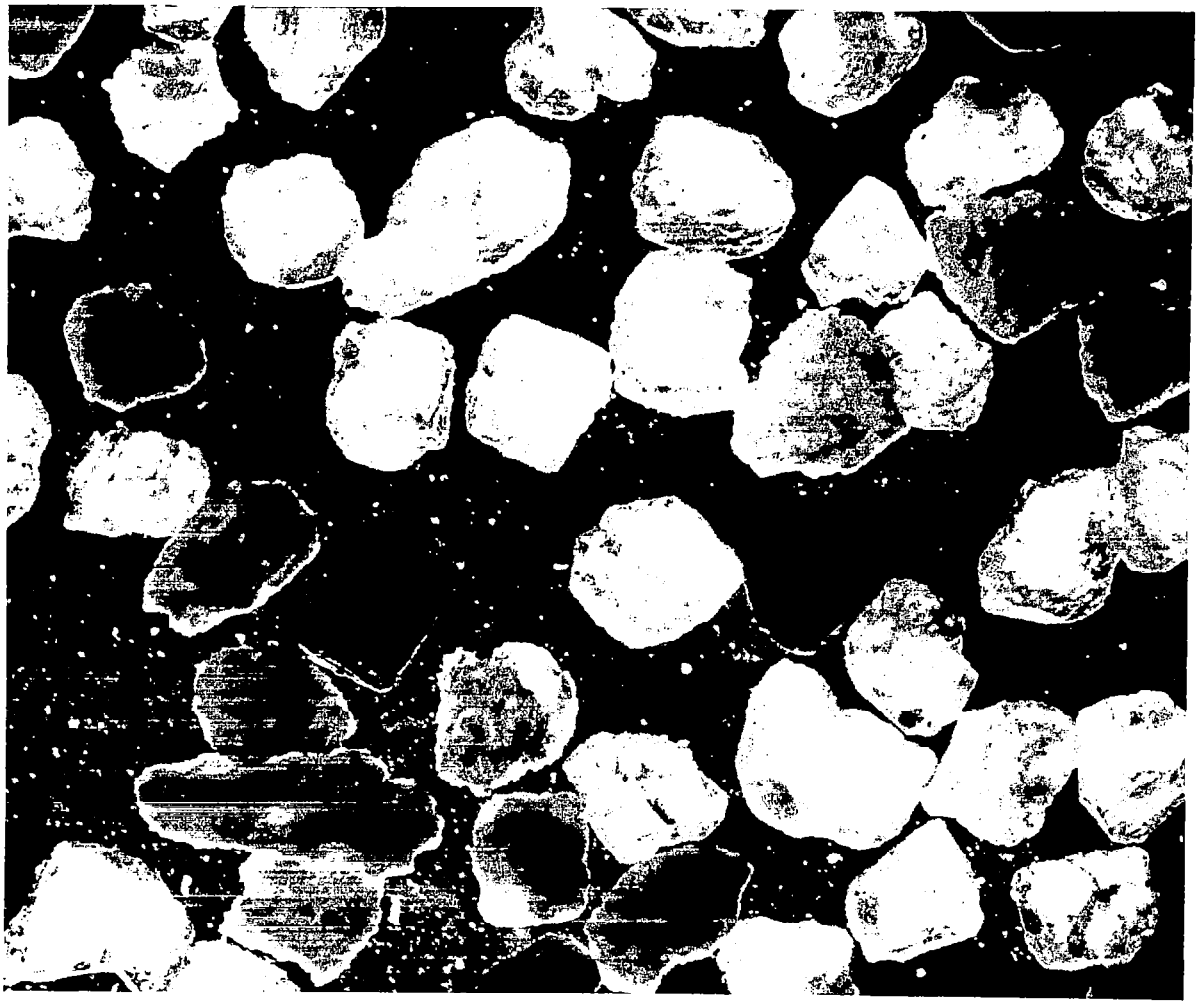

Fig. 8 Fluidized Ash Flow Tuff (590 to 840 Microns)

Table I

MATERIALS USED IN FLUIDIZATION STUDIES

Material	Source
Glass microspheres No. 4000 No. 2332.5	Microbeads, Inc. Jackson, Mississippi
Talc (Steatite)	Liberty Talc Mines, Inc. Sykesville, Maryland
Granite Dust (Granite gneiss)	Boscobel Quarries Manakin, Virginia
FCCU Catalyst Regenerated catalyst (sodium aluminum silicate)	Texaco Inc. Los Angeles Plant Wilmington, California
F-2-25 Catalyst (high alumina) Al_2O_3 28%, SiO_2 71.6%	W. R. Grace and Co. Davison Chemical Division Baltimore, Maryland
Unwelded Ash Flow Tuff From Bandelier Rhyolite Tuff near Totavi, New Mexico	Obtained by Mr. Morris Estes Texaco District Office Albuquerque, New Mexico Sample location recommended by R. L. Smith, USGS and described in reference (16).

apparatus and standard screens which were chosen from the series shown in Table II. For particles smaller than 400 mesh (37 microns), special micro-screens made by Buckbee Mears* (30, 20, 10, and 5 microns) were used. In a number of instances where narrow-size cuts or blends of cuts were used in the fluidization studies, sufficient amounts of material were screened to provide the desired quantities. In the case of granite, it was necessary to grind material in a ball mill to obtain enough of some of the smaller sizes.

Two samples of glass microbeads were obtained (No. 4000 and No. 2332.5). The sieve analyses are given in Tables III and IV. Both are fairly narrow cuts containing predominantly 37 to 30 micron beads with the No. 4000 sample having some material smaller, and the No. 2332.5 having some material both larger and smaller. The No. 2332.5 sample was used as-received for several experiments, and substantial portions were screened to obtain individual narrow cuts to determine the effect of size on certain variables.

The analysis of the No. 325 talc is given in Table V. The major portions were between 44 and 20 microns. No separation was carried out.

The size distribution of the crushed granite dust as-received is shown in Table VI. A synthetic mixture of cuts (Granite Mix No. 1) was prepared to essentially duplicate the size distribution of FCCU catalyst to be described below. The composition of the mix is given in Table VII.

Two samples of synthetic catalyst employed in fluidized beds for petroleum processing were used. The FCCU catalyst (Table VIII) had been regenerated after use in catalytic cracking operations and contained only moderate particle porosity but the particles were well rounded. The size distribution was relatively similar to the new catalyst F-2-25 (Table IX). The new catalyst was of different chemical composition, contained a higher degree of particle porosity, and was more irregular in shape.

The screen analysis for the unwelded-ash-flow tuff is given in Table X. The size distribution in ash flow is of considerable interest. Published data are few, but Moore (17) indicated that the distribution of nuée ardente deposits from the Crater Lake region appeared to follow Rosin's law (18). This law has been of use in the study of crushed materials, especially coal, and is usually given in the form

$$R = 100\, e^{-(x/k)^n}$$

* Buckbee Mears Co., St. Paul, Minn.

Table II

SCREENS USED FOR PARTICLE SIZING

Nominal Dimensions Based on ASTM Fine Series Specifications (E 11-58T)

Size or Sieve (Mesh) Designation		Sieve Opening	
Microns	Number	mm	in.
5660	3-1/2	5.66	0.223
4760	4	4.76	0.187
4000	5	4.00	0.157
3360	6	3.36	0.132
2830	7	2.83	0.111
2380	8	2.38	0.0937
2000	10	2.00	0.0787
1680	12	1.68	0.0661
1410	14	1.41	0.0555
1190	16	1.19	0.0469
1000	18	1.00	0.0394
840	20	0.84	0.0331
710	25	0.71	0.0280
590	30	0.59	0.0232
500	35	0.50	0.0197
420	40	0.42	0.0165
350	45	0.35	0.0138
297	50	0.297	0.0117
250	60	0.250	0.0098
210	70	0.210	0.0083
177	80	0.177	0.0070
149	100	0.149	0.0059
125	120	0.125	0.0049
105	140	0.105	0.0041
88	170	0.088	0.0035
74	200	0.074	0.0029
63	230	0.063	0.0025
53	270	0.053	0.0021
44	325	0.044	0.0017
37	400	0.037	0.0015
	Special Sieves (Buckbee-Mears)		
30	-	0.030	0.0012
20	-	0.020	0.0008
10	-	0.011	0.0004
5	-	0.005	0.0002

Table III

SIEVE ANALYSIS OF NO. 4000 GLASS MICROSPHERES
200 gm sample

Particle Size, μ	Wt. Percent
>53	0
53-44	0.30
44-37	2.10
37-30	76.50
30-20	19.47
20-10	0.97
10-5	0
<5	0

Table IV

SIEVE ANALYSIS OF NO. 2332.5 GLASS MICROSPHERES

Particle Size, μ	Wt. Percent
>62	0.67
62-53	0.35
53-44	1.52
44-37	16.02
37-30	72.50
30-20	9.10
20-10	.48
10-5	0
<5	0

Table V

SIEVE ANALYSIS OF NO. 325 TALC
200 gm sample

Particle Size, μ	Weight Percent
> 88	0.40
88 - 74	0.98
74 - 62	2.03
62 - 53	1.93
53 - 44	7.65
44 - 37	11.55
37 - 30	36.95
30 - 20	31.11
20 - 10	5.15
10 - 5	0
< 5	0

Table VI

SIEVE ANALYSIS OF CRUSHED GRANITE DUST
200 gm sample

Particle Size, μ	Avg. Particle Size, mm	Wt. percent	Cumulative Wt. percent
> 4760	> 4.76	1.15	1.15
4760 - 2000	3.38	25.75	26.90
2000 - 840	1.42	26.70	53.60
840 - 590	0.718	8.25	61.85
590 - 420	0.575	9.80	71.65
420 - 210	0.315	9.90	81.55
210 - 149	0.1795	4.25	85.80
149 - 105	0.127	2.90	88.70
105 - 74	0.0895	2.85	91.55
74 - 63	0.0685	1.50	93.05
63 - 53	0.058	0.20	93.25
53 - 44	0.0485	1.10	94.35
< 44	< 0.044	5.15	99.50

Table VII

COMPOSITION OF GRANITE MIX NO. 1

Particle Size, μ	Weight Percent
125 - 105	1.2
105 - 88	3.2
88 - 74	8.0
74 - 63	14.8
63 - 53	0.9
53 - 44	30.9
44 - 37	12.8
< 37	27.7

Table VIII

SIEVE ANALYSIS OF FCCU REGENERATED CATALYST
200 gm sample

Particle Size, μ	Weight Percent
> 420	0.05
420 - 297	0.08
297 - 250	0.10
250 - 210	0.13
210 - 177	0.10
177 - 149	0.18
149 - 125	0.23
125 - 105	0.60
105 - 88	3.20
88 - 74	7.98
74 - 63	14.53
63 - 53	0.93
53 - 44	30.90
44 - 37	12.68
< 37	27.68

Table IX

SIEVE ANALYSIS OF F-2-25 CATALYST
200 gm sample

Particle Size, μ	Weight Percent
> 297	0
297 - 250	0
250 - 177	0
177 - 149	0.15
149 - 125	0.28
125 - 105	0.93
105 - 88	3.08
88 - 74	7.25
74 - 63	25.03
63 - 53	1.50
53 - 44	17.23
44 - 37	19.43
37 - 30	21.22
30 - 20	2.28
20 - 10	0.48
10 - 5	0
< 5	0

Table X

SIEVE ANALYSIS OF UNWELDED ASH FLOW TUFF
200 gm sample

Particle Size, μ	Avg. Particle Size, mm	Weight, gm	Weight Percent	Cumulative Weight Percent
> 12,700	> 12.7	3.03	1.52	1.52
12,700 - 6,350	9.525	3.48	1.74	3.26
6,350 - 4,760	5.555	3.07	1.53	4.79
4,760 - 2,000	3.380	13.50	6.75	11.54
2,000 - 840	1.420	36.20	18.10	29.64
840 - 590	0.715	16.40	8.20	37.84
590 - 420	0.505	18.80	9.40	47.24
420 - 297	0.3585	10.00	5.00	52.24
297 - 250	0.2735	5.20	2.60	54.84
250 - 210	0.230	5.60	2.80	57.64
210 - 177	0.1935	5.10	2.55	60.19
177 - 149	0.163	7.35	3.68	63.87
149 - 125	0.137	5.20	2.60	66.47
125 - 105	0.115	4.60	2.30	68.77
105 - 88	0.0965	7.70	3.85	72.62
88 - 74	0.0810	7.00	3.50	76.12
74 - 62	0.0680	6.60	3.30	79.42
62 - 53	0.0575	1.70	0.85	80.27
53 - 44	0.0485	7.55	3.78	84.05
44 - 37	0.0405	5.55	2.78	86.83
37 - 30	0.0335	9.13	4.56	91.39
30 - 20	0.0250	6.82	3.41	94.80
20 - 10	0.0150	5.83	2.92	97.72
10 - 5	0.0075	0.22	0.11	97.83
< 5	< 0.005	0.	0.	0.

where R is the weight percent retained on a screen of mesh x, and k and n are constants for any given material.

A good discussion of this law and its application to sediments and the natural disintegration of rock sources by crushing or random breakage of the material is given by Krumbine and Tisdel (19). If the cumulative weight percent is plotted versus particle size, using an empirical scale developed by Geer and Yancy (20), those materials following Rosin's law will give a straight line. This is illustrated by Fig. 9. Crushed granite (Table VI) shows essentially a straight line and follows Rosin's law. The unwelded-ash-flow sample examined in this program, however, does not follow the law. The full range material and a heart cut made by excluding large and small particles (Tables X and XI) both show distinct curvature. They indicate a higher proportion of small-particle size material than would be expected from natural crushing. It is believed possible that this is caused by the relative friability of the porous tuff and the tendency to break more readily into smaller particles during handling and screening.*

4. Physical Measurements of Particles

In addition to particle size, a number of physical measurements were made to help characterize the various particles. Pore volume and surface area were measured by the BET nitrogen absorption method** and the material density (skeletal density) was determined by isopropyl alcohol displacement after drying for 1 hour at 400° C. From these data, the particle densities of porous materials were calculated. Bulk densities were obtained in the fluidization columns. The bulk densities (BD) and resultant void fractions were measured under three bed conditions: packed, settled, and fully expanded. This was done by weighing the materials into a fluidization column of known diameter and measuring the height in the column under the three conditions.

Summary physical data are given in Table XII and the detailed data of bulk density determinations for settled and expanded beds are given in Table XIII.

In the summary table, the pore volumes (cm^3/g) of the three porous materials are shown. This information, together with the material density (solid material

---

* A subsequent screen analysis made with an Allen-Bradley Sonic Sifter under conditions to eliminate any particle breakage shows the same curvature as Fig. 9 and verifies a high proportion of small particles in the ash-flow tuff.

** Brunauer, Emmett and Teller (Ref 21). See also (22) for detailed description.

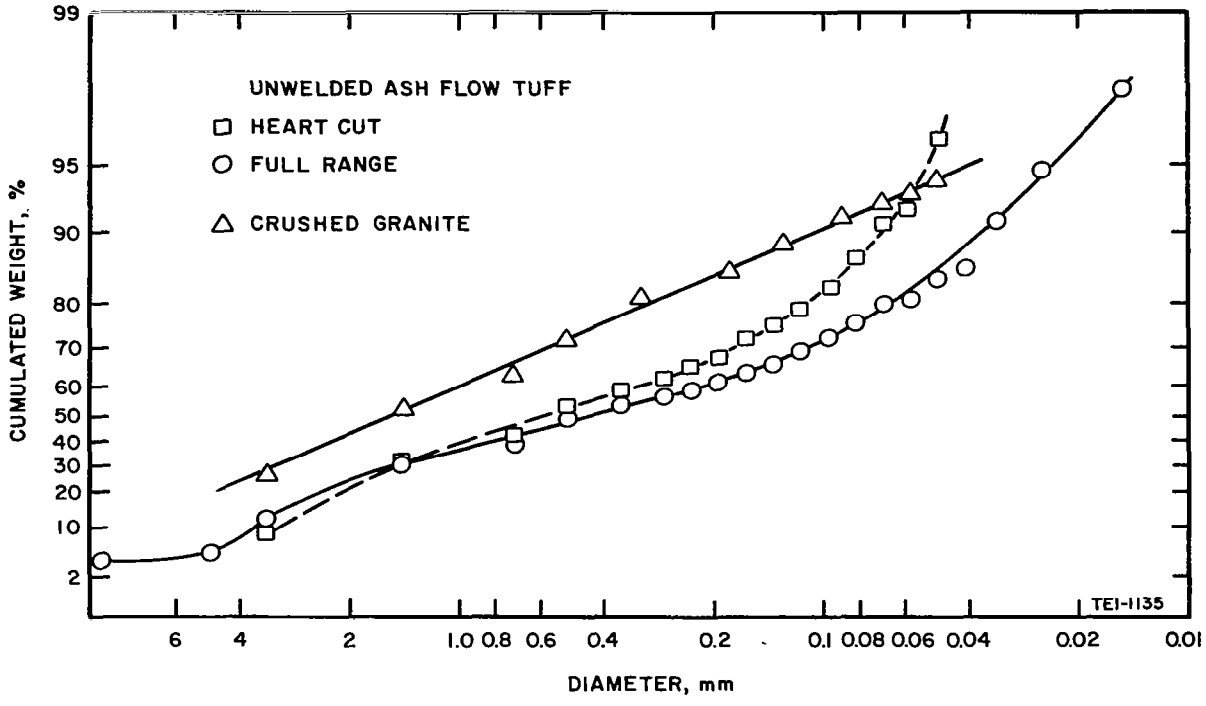

Fig. 9 Rosin's Law Applied to Granite and Ash Flow Tuff

Table XI

SIEVE ANALYSIS OF UNWELDED ASH-FLOW TUFF (HEART CUT)

Adjusted by Removing Very-Large and Very-Small Particles

Avg. Particle Size, mm	Weight, gm	Weight Percent	Cumulative Wt. Percent
3.380	13.50	8.22	8.22
1.420	36.20	22.07	30.29
0.715	16.40	10.00	40.29
0.505	18.80	11.45	51.74
0.3585	10.00	6.09	57.83
0.2735	5.20	3.17	61.00
0.230	5.60	3.42	64.42
0.1935	5.10	3.11	67.53
0.163	7.35	4.49	72.02
0.137	5.20	3.17	75.19
0.115	4.60	2.81	78.00
0.0965	7.70	4.70	82.70
0.0810	7.00	4.26	86.96
0.0680	6.60	4.03	90.99
0.0575	1.70	1.03	92.02
0.0485	7.55	4.60	96.62
0.0405	5.55	3.38	100.00

Table XII

PHYSICAL MEASUREMENTS OF PARTICLES

Material	Particle Size Range Mesh Passes	Mesh Retained on	Microns Smaller than	Microns Larger than	Material Density g/cm³	Pore Volume cm³/g	Particle Voidage	Particle Density g/cm³	Surface Area m²/g	Bulk Density, (BD) and Void Fraction (ε) Packed Bed B.D., g/cm³	Packed Bed Void Fract., ε	Settled Bed B.D., g/cm³	Settled Bed Void Fract., ε	Fully Expanded Bed B.D., g/cm³	Fully Expanded Bed Void Fract., ε	Bed Expansion Ratio
Glass Microspheres No. 2332.5	325		44	20	2.48	0	0	2.48	-	1.37	0.448	1.21	0.513	1.02	0.589	1.19
Talc No. 325, unsized	270		53	10	2.83	0	0	2.83	5.0	0.85	0.700	0.655	0.769	0.373	0.868	1.76
Granite	80	100	177	149								1.07	0.584	0.95	0.63	1.13
	120	140	125	105								1.05	0.592	0.88	0.658	1.19
	140	170	105	88	2.57	0	0	2.57	4.4	1.22	0.525	1.03	0.599	0.85	0.669	1.21
	200	230	74	63								0.98	0.619	0.76	0.704	1.29
	270	325	53	44								0.93	0.638	0.71	0.724	1.31
	325		44									0.90	0.650	0.72	0.72	1.25
Regenerated FCCU Catalyst Unsized	140	400[a]	105	37[a]	2.455	0.28	0.407	1.455	75	0.95	0.347 0.613[b]	0.83	0.430 0.662[b]	0.669	0.540 0.728[b]	1.24
F-2-25 Catalyst	140		105	20	2.358	0.88	0.675	0.767	423	0.51	0.335 0.784[b]	0.448	0.416 0.810[b]	0.269	0.649 0.886[b]	1.67
Unwelded Ash Flow Tuff	120		125	5	2.473	0.06	0.129	2.154	4.3	0.945	0.561 0.618[b]	0.764	0.645 0.691[b]	0.527	0.755 0.787[b]	1.45

(a) 27.7 wt% smaller than 37 microns (passes thru 400 mesh)
(b) Includes voidage in particles as well as between particles

Table XIII

BULK DENSITY (gm/cm^3) OF FLUIDIZED MATERIALS

	No. 2332.5 Glass Microspheres	
	Settled Bed	Expanded Bed
	1.22	1.01
	1.21	1.01
	1.22	1.04
	1.21	1.02
	1.22	1.01
	1.22	1.05
	1.22	1.12
	1.16	0.96
	1.18	0.96
Avg.	1.21	1.02

	No. 325 Talc	
	Settled Bed	Expanded Bed
	0.685	0.392
	0.66	0.37
	0.65	0.366
	0.646	0.364
	0.632	0.374
Avg.	0.655	0.373

	F-2-25 Catalyst (Unsized)	
	Settled Bed	Expanded Bed
	0.448	0.269

	Unwelded Ash Flow Tuff (5-125 μ)	
	Settled Bed	Expanded Bed
	0.785	0.525
	0.764	0.518
	0.755	0.527
	0.767	0.531
	0.750	0.535
Avg.	0.764	0.527

	Regenerated FCCU Catalyst (Unsized)	
	Settled Bed	Expanded Bed
	0.88	0.673
	0.83	0.66
	0.816	0.666
	0.812	0.671
	0.810	0.675
Avg.	0.83	0.669

only) permits calculation of the particle voidage (void fraction in the particle) and the particle density. The F-2-25 catalyst contains 67.5 volume percent voids within the particles and thus has a particle density of only 0.767 g/cm^3. The FCCU catalyst has moderate porosity (40.7 percent) with a particle density of 1.455, and the ash-flow tuff has a lower porosity (12.9 percent) with a density of 2.154. The other materials have no porosity so the particle density is the same as the material density.

The surface area (square meters per gram) is 423 for the porous F-2-25 catalyst and 75 for the FCCU catalyst. Surprisingly, the ash-flow tuff has a surface area of only 4.3, comparable to the granite and talc areas of 4.4 and 5.3, respectively. This may reflect a relatively smooth surface similar to a glazed or glassy material. The area is not necessarily related to porosity and that of the tuff is distinctly different from those of the synthetic catalysts.

The void fraction in settled and expanded beds increases with decreasing particle size. This may be seen in Table XII in the case of granite. The bed expansion ratio also increases with decreasing particle size.

B. SETTLING RATES

One of the first properties to be considered in attempting to define the important flow properties of a fluidized material is that of settling rate. The ability of a material to flow depends to a large extent on how long the material remains in a fluidized state. A knowledge of settling rates, and the factors affecting settling rates, should supply this information. Apparatus used in obtaining settling rate data is shown in Fig. 10. It consists of a vertical glass tube - the fluidizing column - in which the materials are fluidized and the actual settling rates determined, and an associated gas metering system. The fluidization column is 4.8-cm ID and 120-cm long. A fritted glass disc, having a porosity of 25 to 50 microns, sealed into the tube near one end served to support the bed material and to disperse the incoming gas. Gas flow was controlled by sonic orifice flowmeters. These devices deliver a constant mass flow of gas which is dependent only on the upstream pressure of the gas. Variations downstream of the orifice do not affect the mass flow of gas through the orifice so long as the pressure drop across the orifice is at least 2:1. Unless otherwise noted, dry nitrogen was used as the fluidizing medium throughout the investigation. A filter over the upper end of the fluidization column prevented elutriated particles from being discharged into the laboratory. All materials were dried in a vacuum oven before use. In a typical run, a weighed amount of the material under investigation was placed in the fluidization column and the flow of gas through the column gradually increased until the material became fluidized. Gas flow was adjusted to produce maximum expansion of the material without excessive slugging or bubbling. Once stable fluidization of the column was obtained, the gas flow was diverted from the fluidization column by means of a three-way electric solonoid valve and the time required for the column to settle a given distance was determined. Settling rates were obtained from a plot of decrease in column height as a function of time. For each test, the weight of material used, the expanded and settled bed heights, the flow rate of gas, and the settling rate were recorded.

Figure 11 shows typical settling rate plots for the various materials used in this investigation. All measurements were made at 1 atmosphere pressure and at room temperature. Although size distributions vary somewhat from one material to another, the range of sizes is approximately the same for all materials used in Fig. 11. The effect of particle size and size distribution will be discussed in detail later. As can be seen from the graph, settling rates vary considerably from one material to another. For example, glass microspheres have a settling rate of 0.33 cm/sec while granite of comparable size settles at a rate of 1.8 cm/sec. Other materials fall between these values. In general, materials composed of smooth, rounded particles

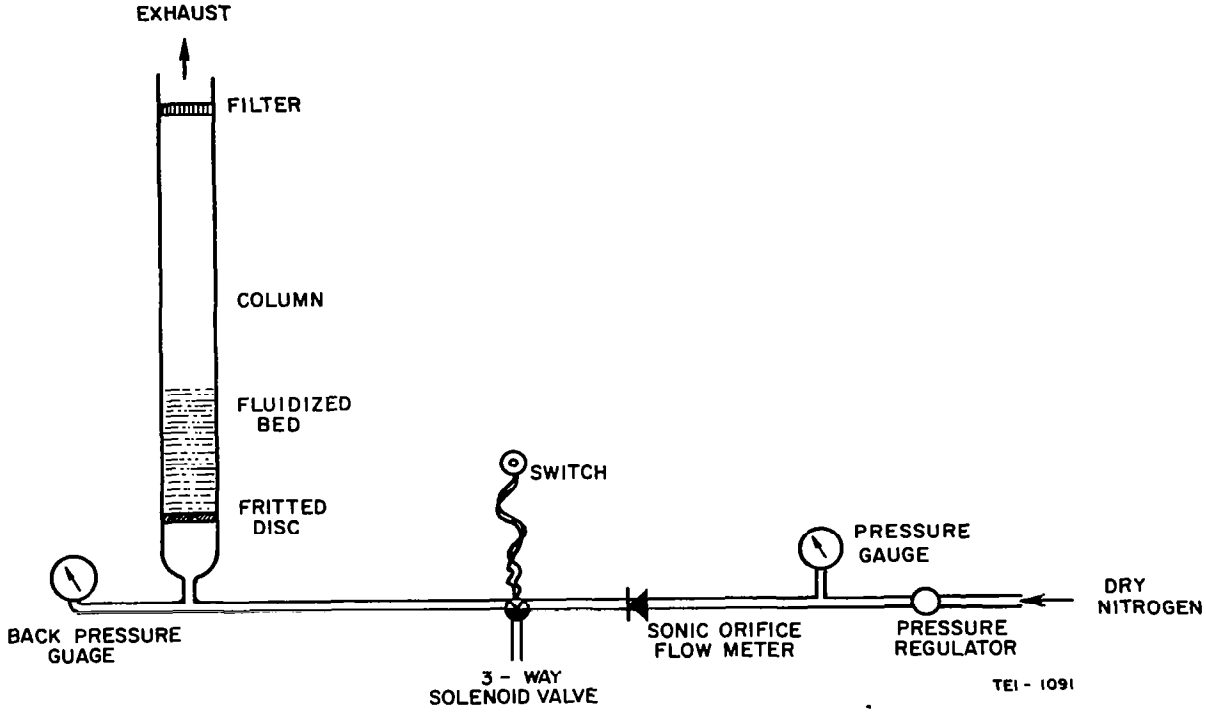

Fig. 10 Experimental Set-up for Studying Settling Rates of a Fluidized Bed

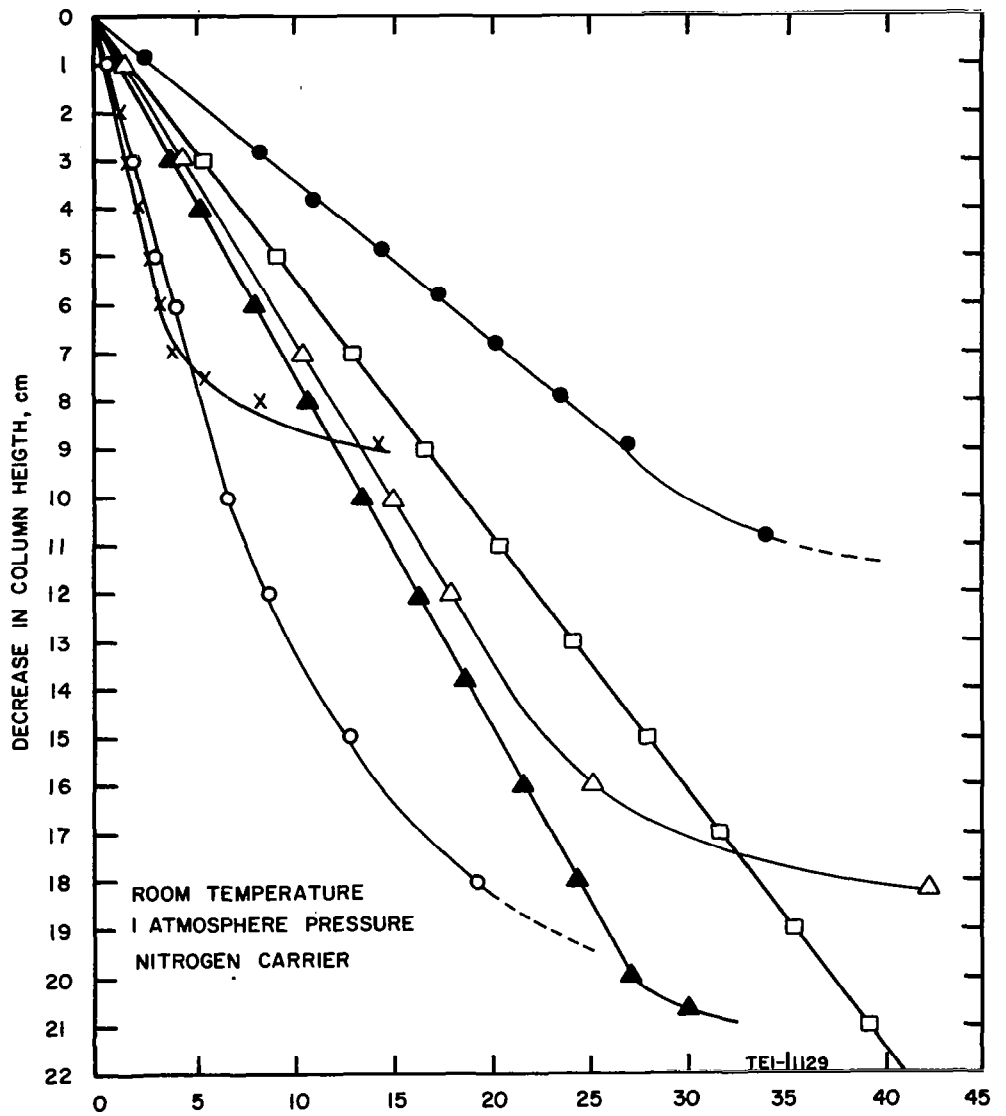

	EXPANSION RATIO	INITIAL SETTLING RATES, cm/sec
● – GLASS MICROSPHERE, NO.4000	1.2	0.33
△ – FCCU CATALYST, UNSIZED	1.3	0.65
o – TALC, NO. 325	1.7	1.6
x – GRANITE, MIX NO.1	1.3	1.8
□ – F-2-25 CATALYST, UNSIZED	1.6	0.55
▲ – ASH FLOW TUFF, < 125 μ	1.4	0.73

Fig. 11 Effect of Particle Shape on Settling Rates

fluidize more uniformly and with greater ease and give slower settling rate than the more irregular, sharp-edged particles. In addition, the settling rates of these materials were linear over most of the settling distance, while in the more irregularly shaped materials (granite and talc), settling rates are rapid at first and decrease with time. This variation in settling rates is apparently related to the manner in which fluidization in these materials occurs. Instead of a uniform fluidization throughout the bed, where each particle is separated from its neighbors, granite and talc particles tended to agglomerate into rather large masses. These larger masses would be expected to have faster settling rates.

One of the conditions necessary for fluidization is that the back pressure of the gas at the bottom of the column must equal the pressure due to the weight of the column. Because of the difficulty of obtaining uniform fluidization of granite particles, several comparisons of back pressure and column pressures were made to determine whether or not conditions were satisfactory for fluidization. In each case tested, the back pressure equaled or slightly exceeded the column. For example, 1000 grams of granite in a 5.0-cm ID column* exerts a pressure of 0.113 lb/cm^2. The back pressure of the fluidizing gas was measured and found to be 0.112 lb/cm^2. The agreement is quite good and indicates the conditions were satisfactory for fluidization of the bed. A plot of back pressure as a function of column weight for granite is shown in Fig. 12. Little dependence was observed on particle size. The pressure gradient in the fluidized granite bed was 0.64-mm Hg per centimeter depth.

The effect of bed depth on settling rates was investigated for a number of different materials. The purpose of these experiments was to determine the feasibility of extrapolating the present data to beds of greater depth. Results obtained with the FCCU catalyst are shown in Fig. 13. The data are quite consistent and show that, with the exception of the very shallow bed, the settling rate of the bed is independent of bed depth. Results also show that expansion ratios (height of expanded column to settled column), which in this case were of the order of 1.3, were also unaffected by bed depth. Similar results were obtained with other materials used.

The effect of column diameter on settling rates is shown in Fig. 14. For the present studies, it was desirable to use as small a diameter column as possible to minimize the amount of material required for the individual tests. At the same time, it was important to use a column large enough in diameter so that wall effects would be insignificant. Comparative tests were conducted in 4.8-cm and 6.3-cm ID columns using glass microspheres as the bed material. No difference in settling rates in the two columns was detected, indicating that the 4.8-cm ID column used in most of the experiments was sufficiently large to eliminate any appreciable wall effects.

* A 5.0-cm ID column was used in early work with granite.

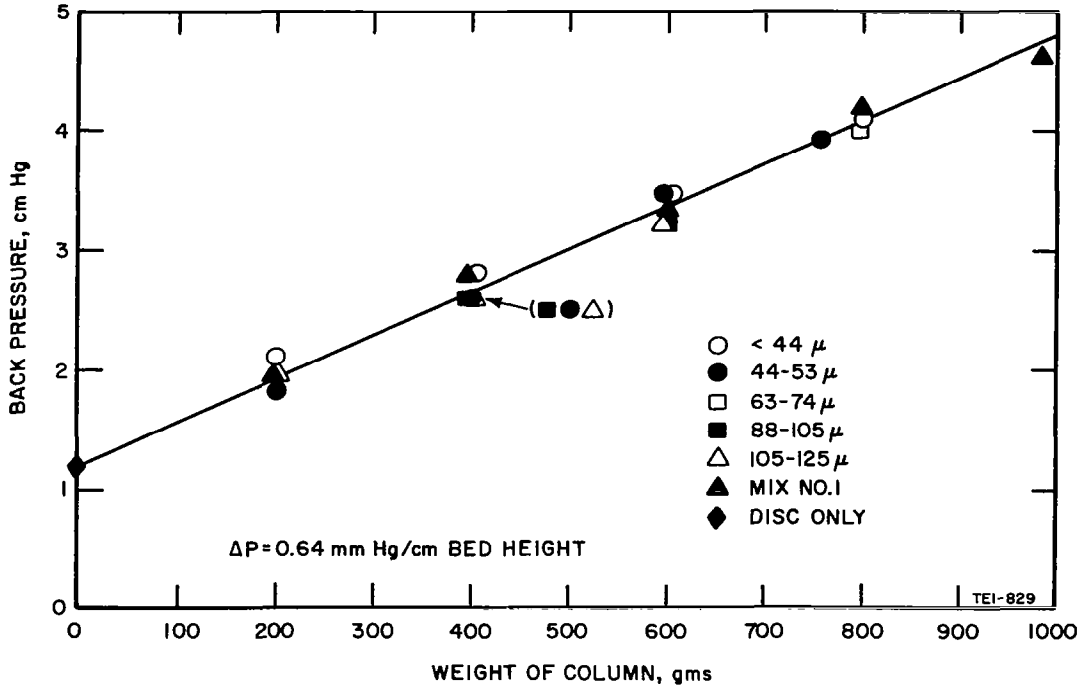

Fig. 12 Effect of Column Weight on Back Pressure of Fluidized Granite Column 4.8-cm ID

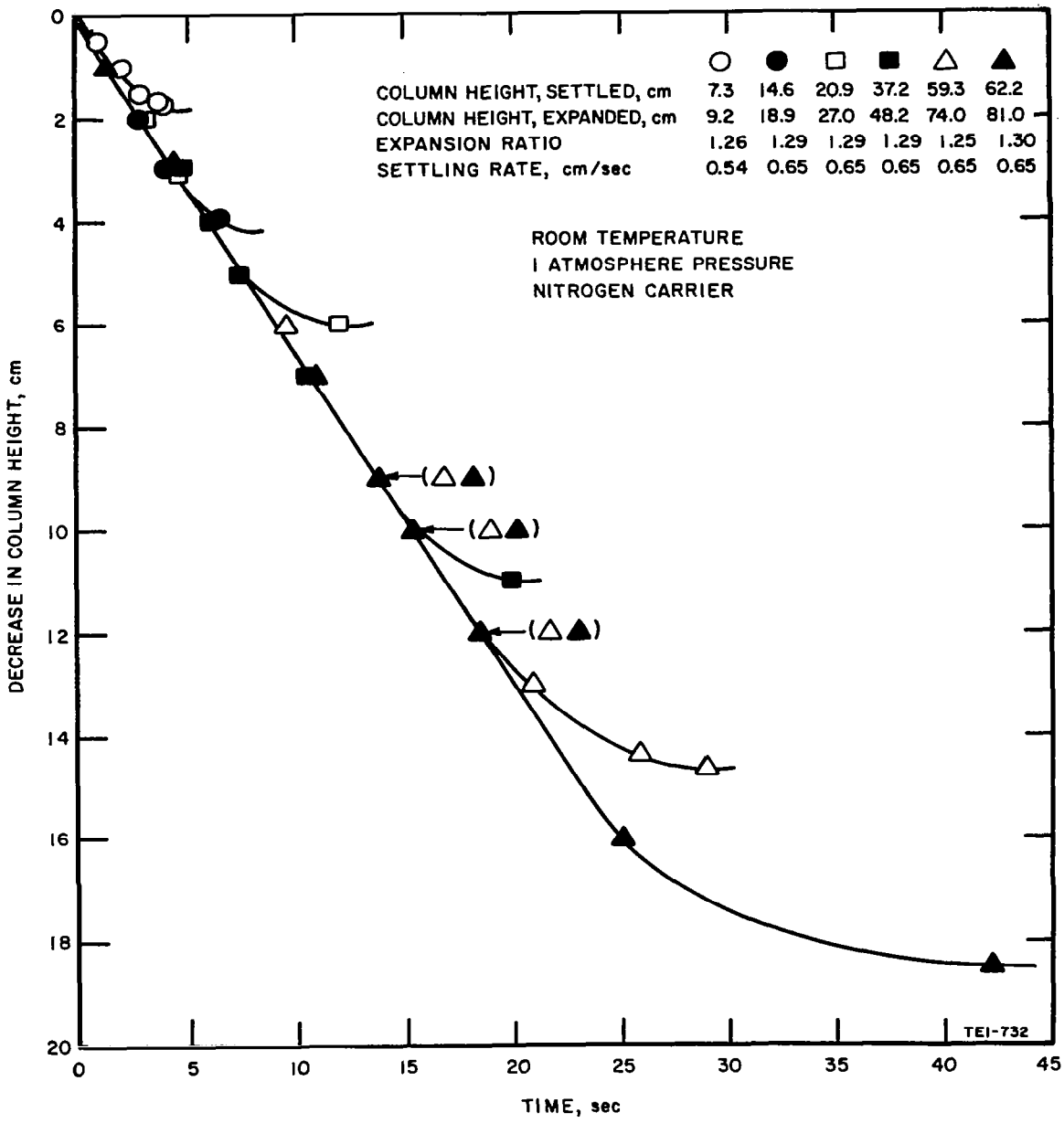

Fig. 13 Effect of Bed Depth on Settling Rate of Unsized FCCU Catalyst

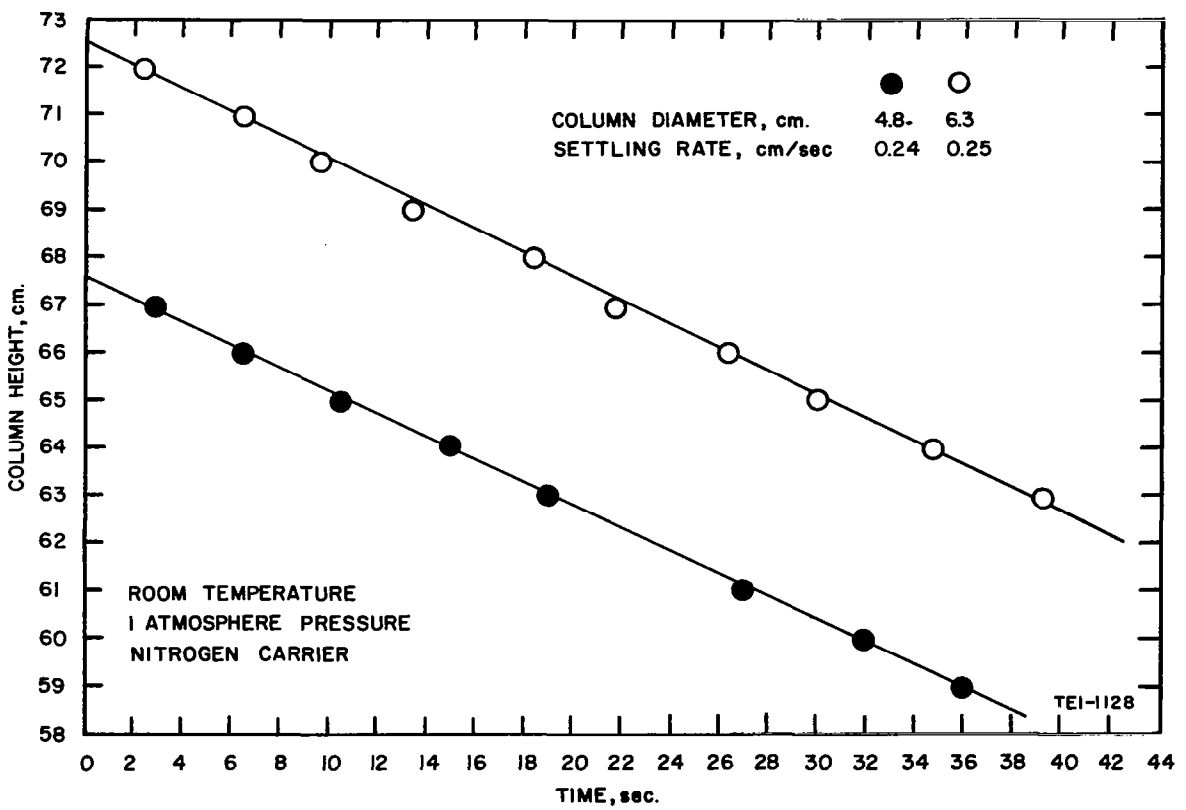

Fig. 14 Effect of Column Diameter on Settling Rates
(Bed Material No. 2332.5 Glass Microspheres)

Figure 15 shows the effect of bed expansion on settling rates. For a given bed, it is possible to control the amount of bed expansion to some extent by regulating the flow of the fluidizing medium. When the pressure drop across the bed is equal to the weight of the bed, the bed becomes fluidized. Further increases in flow cause additional bed expansion. At some point, expansion will cease and large gas bubbles will begin to form in the bed and rise to the surface, producing a rather violent boiling or slugging effect. In determining settling rates, it is important to know the effect of bed expansion on these rates. Figure 15 shows the results of this study. Glass microspheres were used as the bed material. Below the point at which slugging occurs, settling rates are linear over most of the settling distance and increase slightly with increasing expansion. When the bed is expanded to the point of slugging, the settling rate is quite rapid at first and decreases with time. Thus, in studying settling rates, it is important to know the expansion ratio for which the settling rate was determined. Unless otherwise stated, all settling rates in this investigation were determined at maximum bed expansion without slugging.

The effect of changing the fluidizing medium is shown in Fig. 16. Here, nitrogen was replaced with argon and the effect on settling rates determined. Settling rates in an argon atmosphere were faster than those in a nitrogen atmosphere (0.43 cm/sec for argon compared with 0.37 cm/sec for nitrogen). These results are in general agreement with Leva's equation (23) and indicates that a greater mass flow of argon is required to fluidize a given bed than nitrogen.

According to Leva, the minimum flow rate G_{mf} (gm/cm^2-sec) to fluidize a powder is given by:

$$G_{mf} = \frac{1.09 \times 10^{-3} \; D_p^{1.82} \; (\rho_f \, \rho_s \, g \;)^{0.94}}{\mu^{0.88}}$$

. . . . where D_p is the particle diameter (cm), ρ_f is the density of the fluid (gm/cm^3), ρ_s is the density of the solid particle, g is the acceleration of gravity (cm/sec^2), and μ is the viscosity of the fluid (poises = gm/cm-sec). For a given powder, this reduces to

$$G_{mf} \cong \frac{K \, \rho_f^{\,0.94}}{\mu^{0.88}}$$

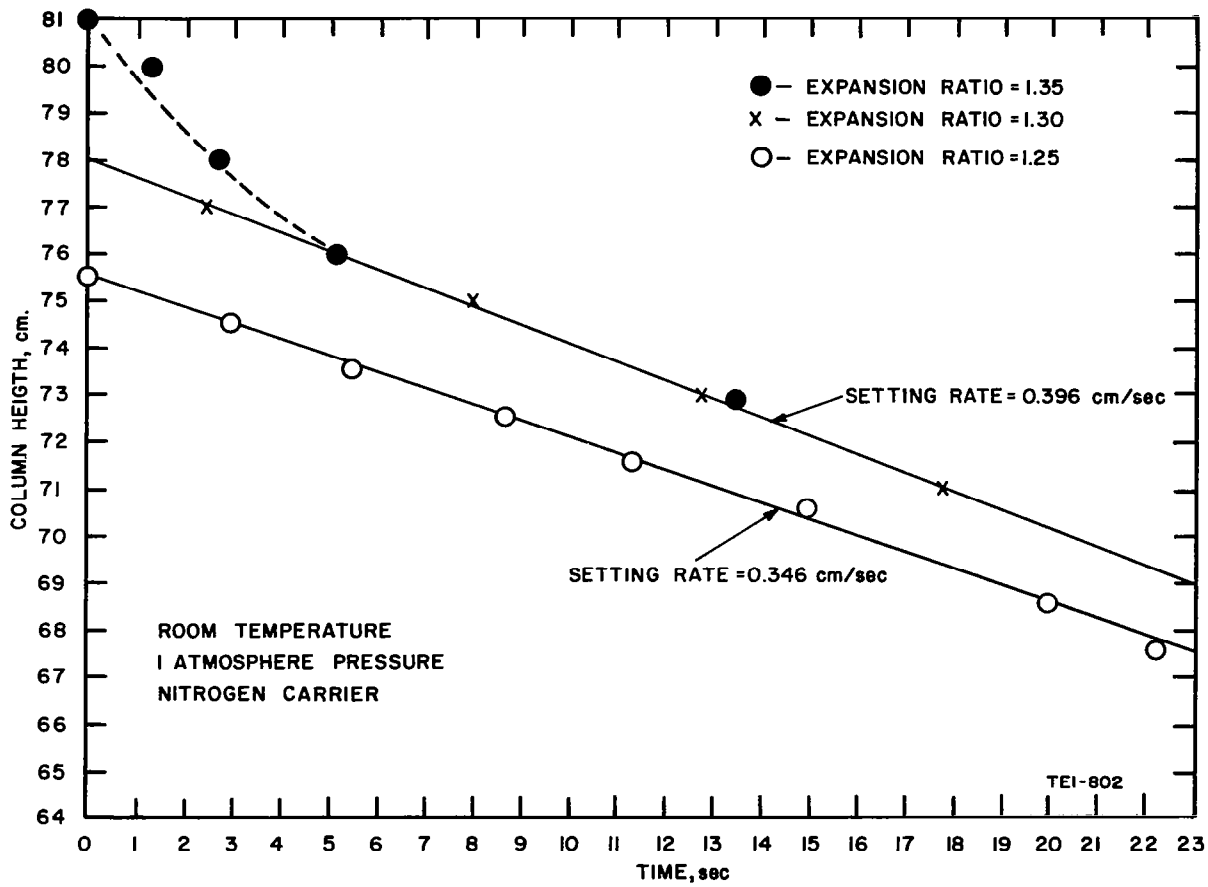

Fig. 15 Effect of Bed Expansion on Settling Rates
(Bed Material No. 4000 Glass Microspheres)

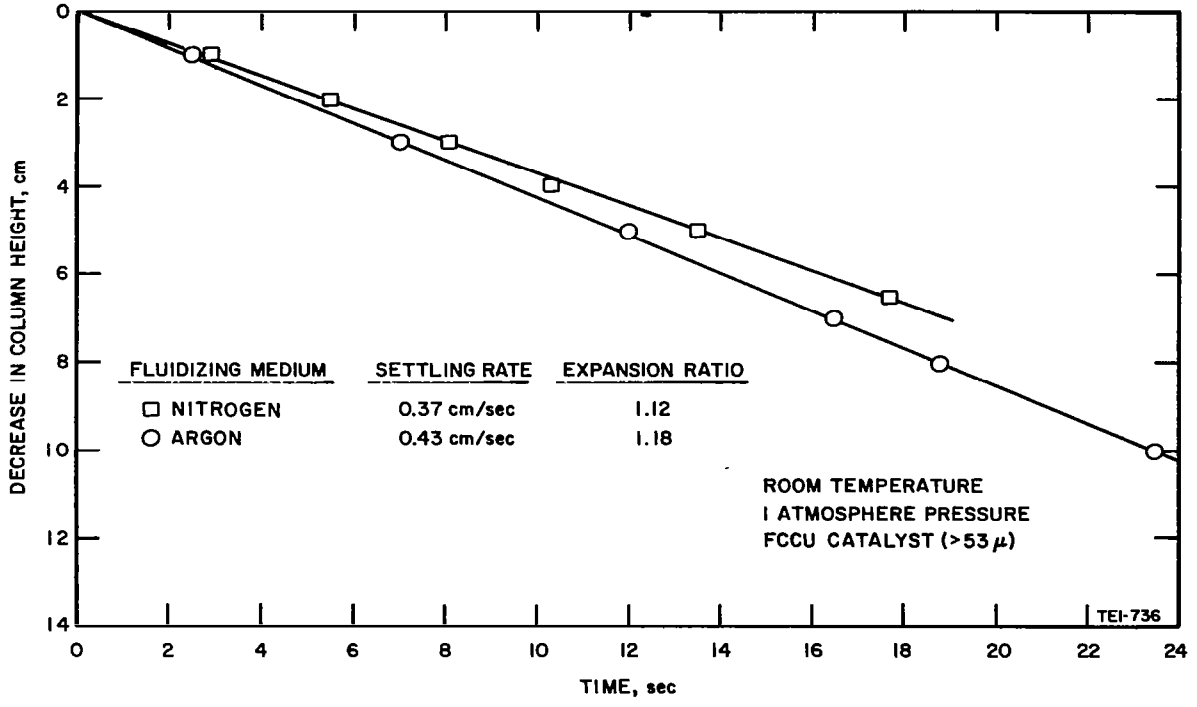

Fig. 16 Effect of Fluidizing Medium on Settling Rates

Using the values at 25°C:

$$\rho_f = 1.146 \times 10^{-3} \text{ gm/cm}^3 \text{ and } \mu = 177.8 \times 10^{-6} \text{ poises for nitrogen}$$

$$\rho_f = 1.634 \times 10^{-3} \text{ gm/cm}^3 \text{ and } \mu = 226.2 \times 10^{-6} \text{ poises for argon}$$

we find that the ratio

$$\frac{G_{mf}\,(\text{nitrogen})}{G_{mf}\,(\text{argon})} = \frac{(\rho_n)^{0.94}\ (\mu_a)^{0.88}}{(\rho_a)^{0.94}\ (\mu_n)^{0.88}} = \left[\frac{1.146}{1.634}\right]^{0.94} \left[\frac{2.262}{1.778}\right]^{0.88} = 0.885$$

This means that a greater mass flow of argon is required to fluidize a given bed than nitrogen. This would imply that the settling rate in argon should be faster than the settling rate in nitrogen. This was found to be the case. The ratio of settling rates, S_R, determined experimentally, is:

$$\frac{S_R\,(\text{nitrogen})}{S_R\,(\text{argon})} = \frac{0.37 \text{ cm/sec}}{0.43 \text{ cm/sec}} = 0.86$$

The agreement is quite good.

Leva's equation, as given above, relates the minimum mass flow for fluidization to particle size. It is of interest to compare the minimum mass flow and also the mass flow actually used to maintain steady fluidization (with near maximum bed expansion) with particle size. This has been done with the glass microspheres and with unwelded ash-flow tuff, using nitrogen gas at 25°C and 1 atmosphere. Employing a glass particle density of 2.48 gm/cm, and the nitrogen density and viscosity previously stated, the expression for the microspheres reduces to:

$$G_{mf} = 5.697\ D_p^{1.82}$$

The calculated minimum flow rate for five sizes of spheres, the experimentally determined minimum flow, and the actual flow rate to maintain expanded bed fluidization are tabulated in Table XIV and the results shown graphically in Fig. 17. The minimum flow was determined by gradually increasing the gas flow through the settled bed until the observed pressure drop no longer increased. At this point, the bed just began to expand. Minimum flow was measured with only two sizes of particles, but results were repeated several times and the values checked very well. The measured G_{mf} for the two sizes agree fairly well with the calculated values and the two curves have the same shape.

Table XIV

MINIMUM MASS FLOW RATE FOR FLUIDIZATION OF GLASS MICROSPHERES

Nitrogen gas, 25°C, 1 atmosphere

$$G_{mf} = \frac{1.09 \times 10^{-3} \; D_p^{1.82} \; (\rho_f \, \rho_s \, g)^{0.94}}{(\mu)^{0.88}}$$

$$D_p = \frac{1.09 \times 10^{-3} \; D_p^{1.82} \left[(1.146 \times 10^{-3}) \; (2.48) \; (979.960)\right]^{0.94}}{(177.8 \times 10^{-6})^{0.88}}$$

$$G_{mf} = 5.697 \; D_p^{1.82}$$

Microsphere Size, μ	Avg. Size, D_p cm x 10^{-4}	$D_p^{1.82}$ cm x 10^{-4}	Calc. G_{mf} g/cm^2 - sec x 10^{-3}	Measured G_{mf} Min. Flow g/cm^2 - sec x 10^{-3}	Measured G Max. Exp. g/cm^2 - sec x 10^{-3}
125 - 105	115	2.95	1.68	1.24	2.55
88 - 74	81	1.56	0.889	-	1.52
74 - 63	69	1.17	0.667	0.494	1.06
44 - 37	41	0.454	0.259	-	0.656
below 37	(30)	0.251	0.146	-	0.559

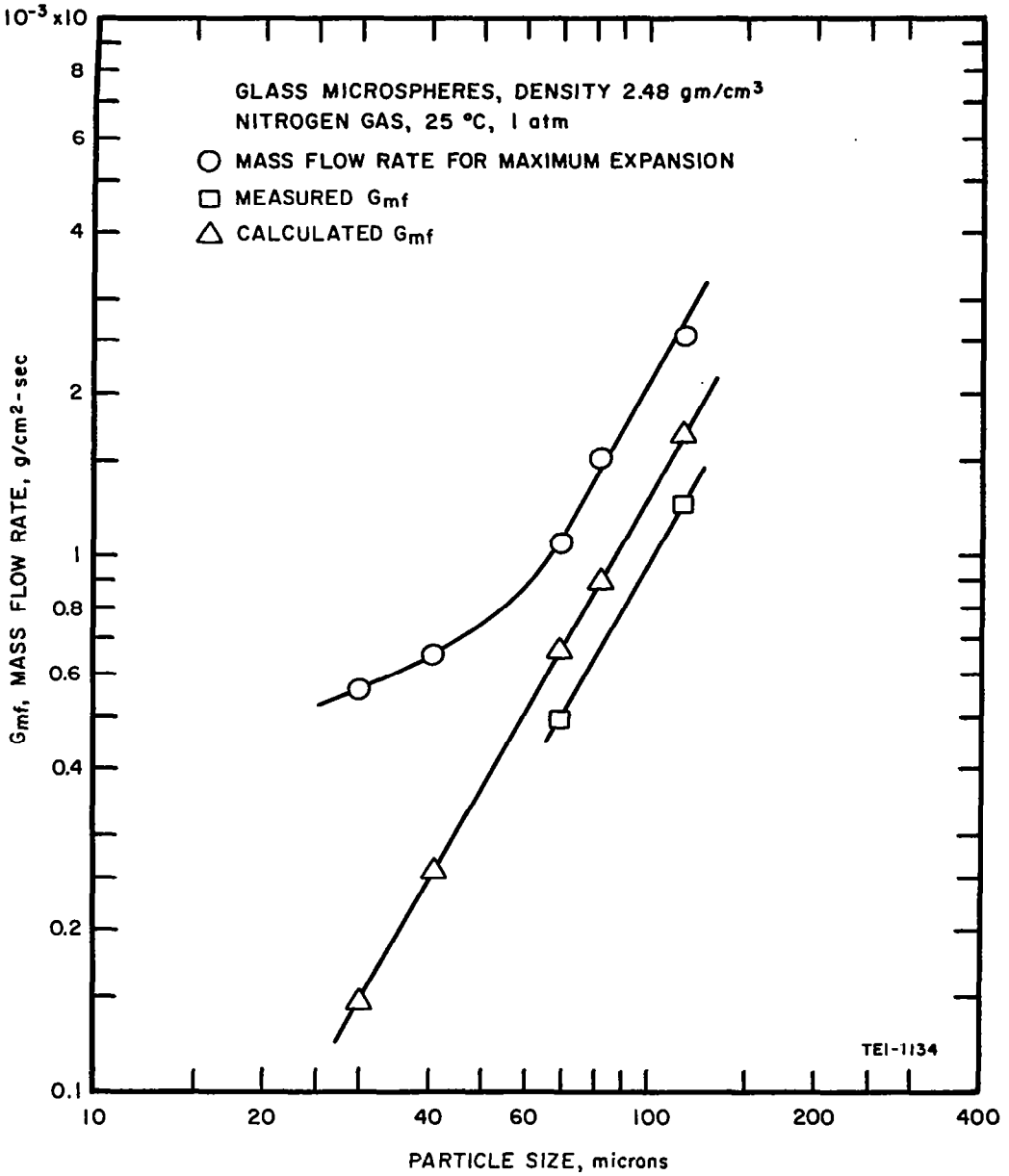

Fig. 17 Minimum Mass Flow Rate (G_{mf}) as a Function of Particle Diameter - Glass Microspheres

In the case of the flow to maintain maximum expansion, the curve for the larger size particles appears to follow the same slope and relationship, but for smaller sizes, the agreement is less satisfactory and this is believed to be caused by the tendency for the smaller particles to agglomerate. Under these circumstances, individual particle size tends to lose its meaning. This has been observed by others (24) who report that for synthetic cracking catalyst, the 10 μ size has severe cohesion and balling, the 25 μ size has cohesion but balling is not too apparent, and that the 40 μ size and above gives good fluidization.

Similar results are shown with the unwelded ash-flow tuff. Using a particle density of 2.154 g/cm^3, the minimum mass flow becomes:

$$G_{mf} = 4.990\ D_p^{1.82}$$

The calculated G_{mf}, the measured G_{mf}, and the mass flow for maximum expansion are shown in Table XV and Fig. 18. For the two values of measured minimum flow, the agreement with the calculated values is excellent. Once again the flow to maintain maximum expansion appears to follow the same general slope for larger particles but deviates appreciably at smaller sizes, presumably due to agglomeration.

It is interesting to compare the flow rates for the irregularly shaped ash-flow particles to the spherical-glass particles. Although the calculated G_{mf} for ash flow is less than that for the glass because of the lower particle density, the measured G_{mf} required and the measured mass flow for expanded bed is greater for the ash flow. Using the data for the larger particle size (115 μ), where the correlation appears best, it may be seen that the ratio for G_{mf} of ash flow to glass spheres is 1.533/1.24 = 1.24 and the ratio of G (expanded bed) for ash flow to glass spheres is 3.2/2.55 = 1.25. It may also be noted that the ratio of mass flow for the fully expanded bed to the minimum flow for the ash flow is 3.2/1.533 = 2.09 and for the glass spheres is 2.55/1.24 = 2.05. The various ratio for smaller size particles differ from the above, possibly because of agglomeration problems.

One might expect a similar relationship to hold between settling rates and particle diameter, although the results are known to be affected to some extent by the amount of expansion of the bed.

Results of studies of the effect of particle size on settling rates are shown for glass microspheres (Table XVI) for ash-flow tuff (Table XVII), and for granite (Table XVIII). The results for spheres and ash flow are plotted in Fig. 19, along with the slope of the curves for calculated G_{mf} from previous

Table XV

MINIMUM MASS FLOW RATE FOR FLUIDIZATION
OF UNWELDED ASH-FLOW TUFF

Nitrogen gas, 25°C, 1 atmosphere
Particle density 2.154 g/cm^3

$$G_{mf} = 4.990\ D_p^{1.82}$$

Particle Size, μ	Avg. Size, D_p cm x 10^{-4}	$D_p^{1.82}$ cm x 10^{-4}	Calc. G_{mf} g/cm^2-sec x 10^{-3}	Measured G_{mf} Min. Flow g/cm^2-sec x 10^{-3}	Measured G Max. Exp. g/cm^2-sec x 10^{-3}
125 - 105	115	2.95	1.47	1.533	3.2
74 - 63	69	1.17	0.585	0.621	1.81
53 - 44	49	0.625	0.312	--	1.09
44 - 37	41	0.454	0.226	--	1.09
< 37	(30)	0.251	0.125	--	0.845

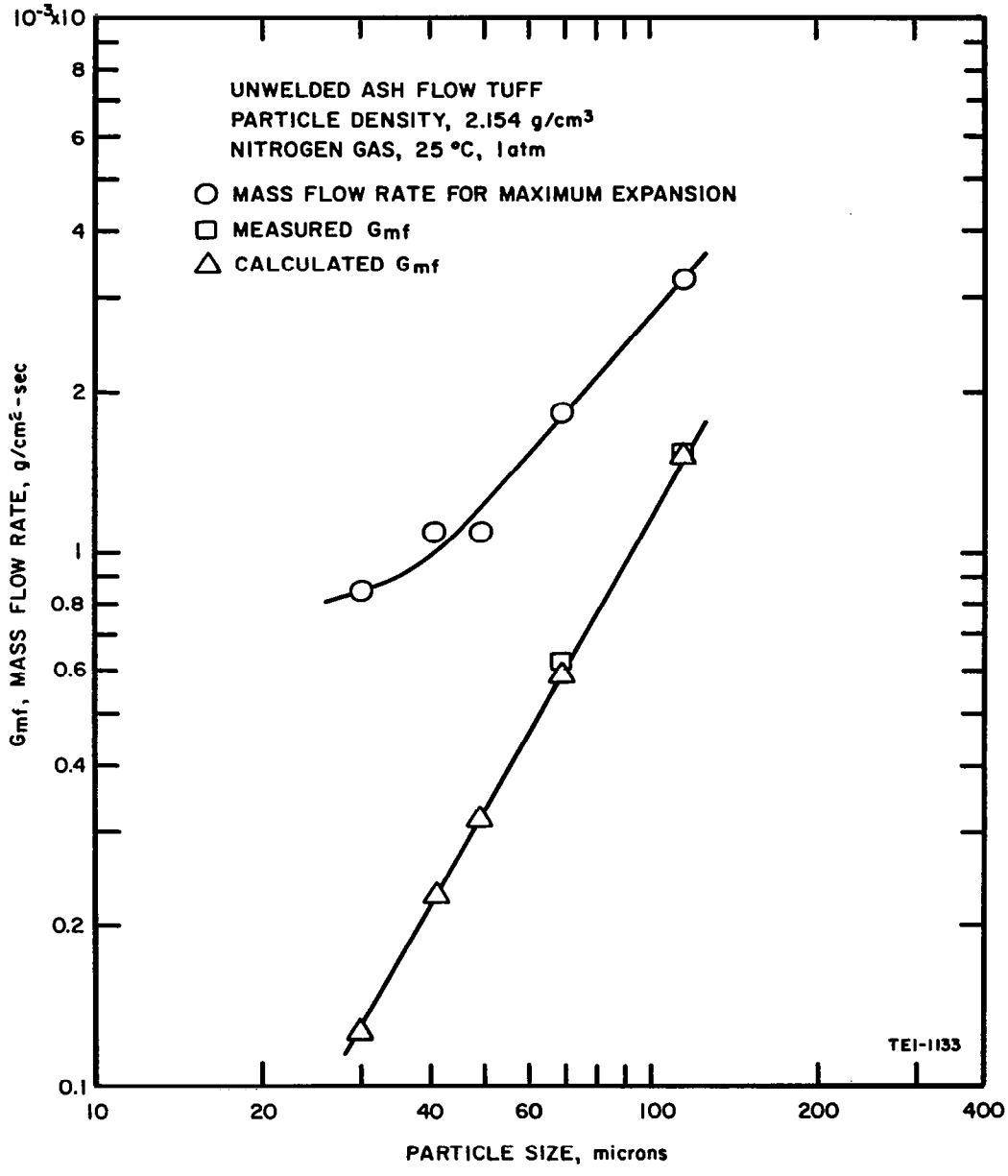

Fig. 18 Minimum Mass Flow Rate (G_{mf}) as a Function of Particle Diameter - Unwelded Ash Flow Tuff

Table XVI

EFFECT OF PARTICLE SIZE ON SETTLING RATE OF GLASS MICROSPHERES

Particle Size,	Settling Rate, cm/sec
125 - 105	1.75
88 - 74	1.20
74 - 63	0.75
44 - 37	0.53
less than 37	0.36

Room temp., N_2 carrier, 1 atm pressure

Table XVII

EFFECT OF PARTICLE SIZE ON SETTLING RATES OF UNWELDED ASH-FLOW TUFF

Particle Size,	Settling Rate, cm/sec
125 - 105	2.0
74 - 63	0.86
53 - 44	0.76
44 - 37	0.72
less than 37*	1.0

Room temp., N_2 carrier, 1 atm pressure

* did not fluidize well

Table XVIII

EFFECT OF PARTICLE SIZE ON SETTLING RATE OF CRUSHED GRANITE

Particle Size,	Settling Rate, cm/sec
125 - 105	1.6
74 - 63	1.6
53 - 44	1.8
less than 44	2.2
Mix No. 1	1.8

Room temp., N_2 carrier, 1 atm pressure

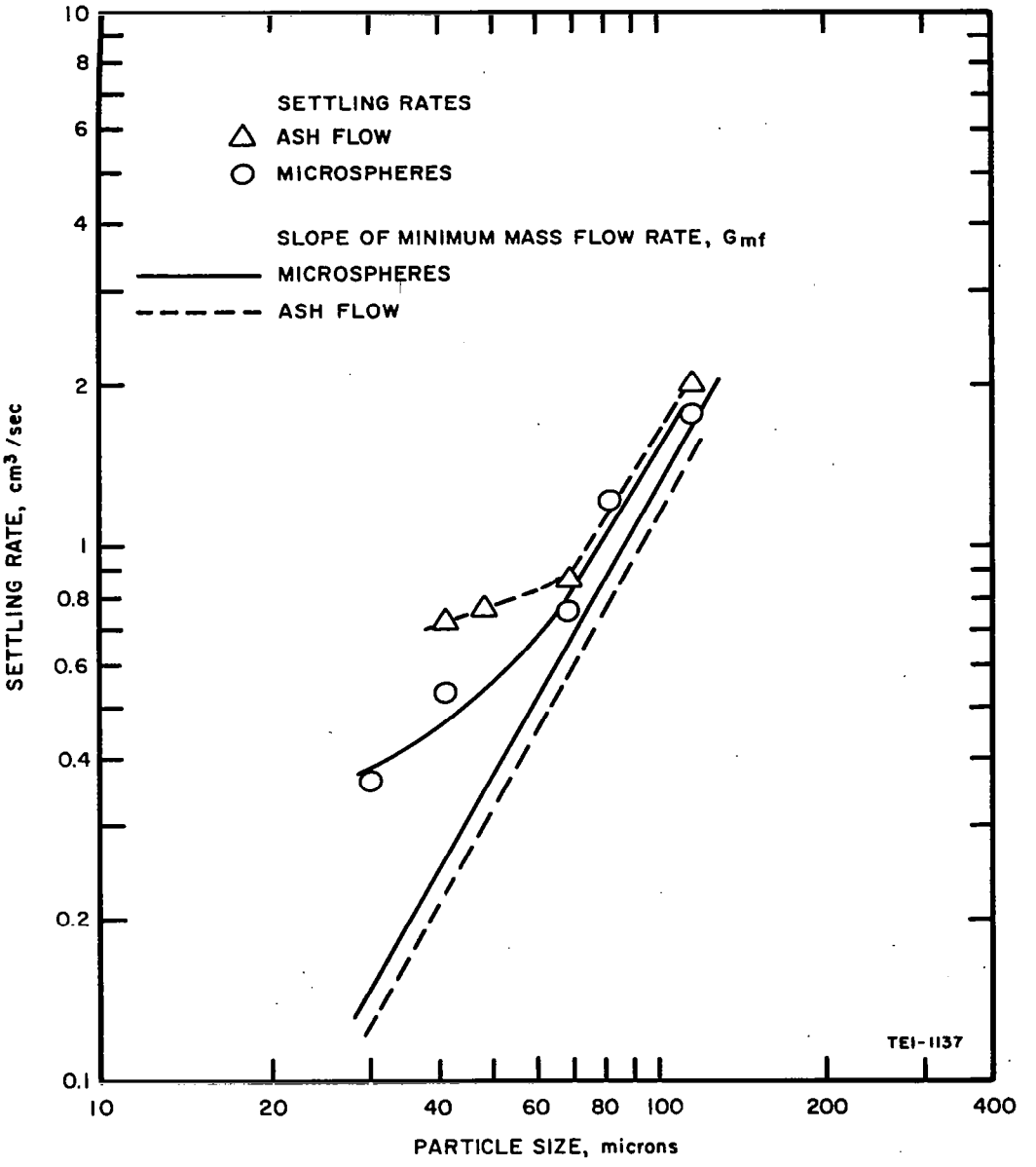

Fig. 19 Effect of Particle Size on Settling Rate

Figures 17 and 18. As would be expected, settling rates decrease with particle size. The slopes of the curves are generally similar, with fair agreement for larger sizes, but more divergence with the smaller particles. This is again believed due to the tendency for small-particle agglomeration and, in the case of glass at least, is abetted by the hygroscopic nature of glass which caused some difficulty in obtaining reproducibility of results and necessitated careful drying of the material before each test.

In the case of granite, Table XVIII, no particular difference in settling rates as a function of particle size is apparent. This, as in the case of the small particles of ash-flow tuff, is probably caused by the irregular shape of the particles causing them to agglomerate.

The effect of size distribution on settling rates of unwelded ash-flow tuff is shown in Table XIX. All particles 125 microns and less in diameter were separated from a fairly large sample of ash-flow tuff and used as the bed material in these experiments. Settling rates of the material were determined as the smaller particles were removed from the sample. The importance of the smaller particles is obvious. As they are removed from the sample, the settling rate of the sample increases. Oddly enough, the settling rate of the smaller particles - less than 37 microns - alone is appreciably higher than when larger particles are also present. Larger particles tend to prevent agglomeration of the smaller particles and in so doing, increase the effectiveness of the smaller particles in controlling the settling rate. Table XX shows how size distribution affects the expansion ratio of the same sample of ash-flow tuff. Removal of the smaller particles cause a reduction in the expansion ratio. Again, the importance of small particles in a sample is obvious.

The effect of particle size on the expansion ratio of unwelded ash-flow tuff is shown in Table XXI. This type of information, coupled with settling rate data, is of value in determining the length of time required for a fluidized column to settle or the length of time available for the material to flow in a fluidized state. As indicated in the table, expansion ratio increases as particle size decreases.

Table XIX

EFFECT OF SIZE DISTRIBUTION ON SETTLING RATES OF UNWELDED ASH-FLOW TUFF

Particle Size, μ	Settling Rate, cm/sec
125 - 37	0.86
125 - 53	1.00
125 - 74	1.34

Table XX

EFFECT OF SIZE DISTRIBUTION ON EXPANSION RATIO OF UNWELDED ASH-FLOW TUFF

Particle Size, μ	Expansion Ratio
125 - 5	1.45
125 - 37	1.22
125 - 53	1.12
125 - 74	1.09

Table XXI

EFFECT OF PARTICLE SIZE ON EXPANSION RATIO OF UNWELDED ASH-FLOW TUFF

Particle Size, μ	Expansion Ratio
125 - 105	1.10
74 - 63	1.16
53 - 44	1.20
44 - 37	1.31
< 37	1.50

C. FLOW PROPERTIES

1. Horizontal Flow Velocities

While settling rate studies are useful in determining the length of time required for a fluidized bed of material to settle, and hence the time available for the material to flow, some knowledge of the horizontal flow properties of the material is required before attempting to predict how far a given material will flow under a given set of conditions. With this in mind, an apparatus was constructed which permitted a measure of horizontal flow velocity and, at the same time, gave a comparative measure of the distance various materials would flow under identical conditions. The apparatus was similar to that used in the settling rate studies, except that the fluidization column was equipped with a removable bottom. The removable section housed the gas dispersion or fluidizer unit and was designed to fit flush with the bottom of the fluidization column. The unit was connected to the flow control system by means of a flexible hose. The fluidization column, a 4.8-cm ID glass tube, was mounted vertically above a large plywood tray on which a grid had been painted to aid in determining distance of travel of the flowing material. A high-speed motion picture camera, mounted above and to one side of the tray, was used to photograph the material as it flowed across the plane. A sketch of the apparatus is shown in Fig. 20.

In actual operation, the fluidizer unit was placed in position and the material to be tested was added to the glass tube. The gas flow was turned on and adjusted until good fluidization of the material was obtained. With the motion picture camera operating, the fluidizer unit was quickly removed from the bottom of the tube, allowing the fluidized material to fall onto the plywood tray. The resulting flow of material across the tray was photographed and the flow velocity determined. Results of the measurements are summarized in Table XXII. In all cases, the depth of the settled bed was approximately the same (35 cm). Most of the measurements were made with the lower end of the glass fluidizer column 11 cm above the tray. In the case of the F-2-25 catalyst, this distance was reduced to 5 cm to prevent the material from flowing completely across the tray and bouncing off the walls. Even with the reduced height, this material traveled across the plane with a velocity of 107 cm/sec, equal to the fastest velocity obtained with the other materials at a drop height of 11 cm. The effect of drop height - the height of the bottom of the glass tube above the tray - can be seen by comparing the flow velocities of the -44 micron diameter granite at drop heights of 11 and 20.5 cm. At

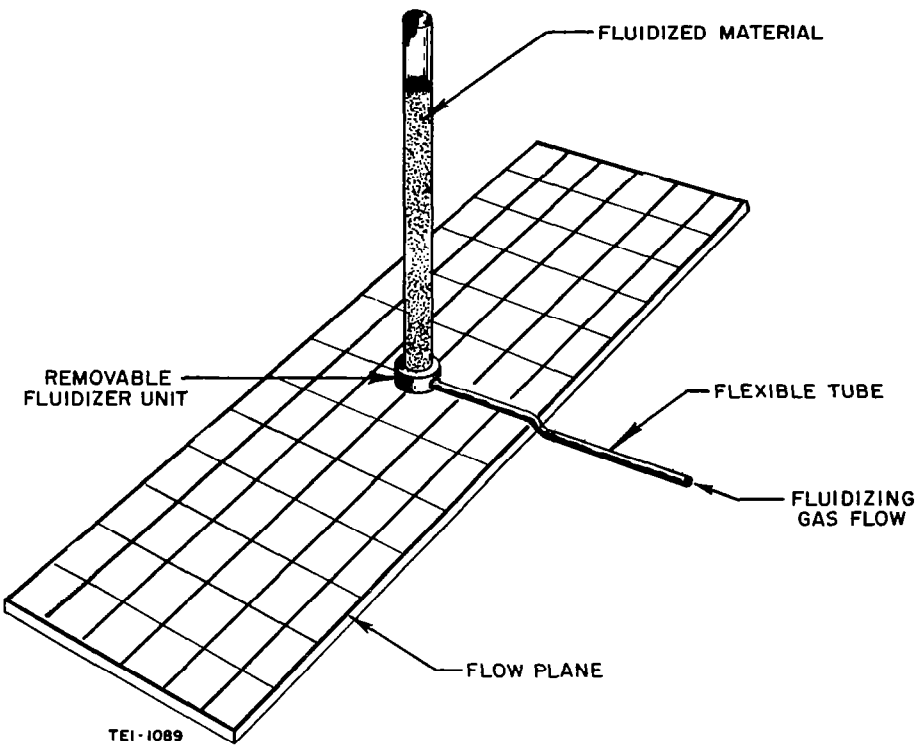

Fig. 20 Experimental Set-up for Determining Flow Properties of Fluidized Materials

Table XXII

HORIZONTAL FLOW VELOCITIES

Material	Flow Velocities, cm/sec	
	11 cm drop height	
	Fluidized	Unfluidized
Granite - less than 44μ	46	27
Granite - 88 - 74μ	53	25
No. 325 Talc	91	23
FCCU - less than 37μ	80	
greater than 37μ	71	
Ash Flow Tuff - less than 125μ	107	40
	5 cm drop height	
F-2-25 - unsized	107	32
	20.5 cm drop height	
Granite - less than 44 μ	128	80 (1) 60 (2)

(1) Velocity for first 5 cm of travel
(2) Velocity for first 10 cm of travel

11 cm, the flow velocity was 46 cm/sec, while at 20.5 cm the velocity increased to 128 cm/sec. Although particle size had a relatively minor effect on flow velocity over the range of sizes investigated, the results observed in granite were contrary to what one might expect and to the results obtained with the FCCU catalyst. That is, the larger granite particles showed a slightly higher flow velocity than the smaller ones. This is probably due to the tendency of the smaller granite particles to agglomerate. Flow velocities of the unfluidized materials are also included in the table. As might be expected, there is a considerable difference in the flow velocities of the fluidized and the unfluidized materials. The F-2-25 catalyst exhibits the highest flow velocity of any of the materials tested with the unwelded ash-flow tuff in second place and the talc in third place.

2. Flow Distances

In addition to the actual flow velocities of the various materials, it is important to know something about the distance these same materials will flow under identical conditions. Such information, combined with settling rate data and flow velocities, should tell a great deal about the characteristics and properties of fluidized flow. The apparatus used for these determinations was the same as that described above, except that the plane was tilted at a slight angle in order to determine the effect of incline on flow. The material was fluidized in the usual manner, the fluidizer removed, and the material allowed to fall and spread across the plane. Dimensions of the flow pattern were obtained. Maximum distances down the plane as well as across the plane were recorded. Results are summarized in Table XXIII. All tests were made under as nearly identical conditions as possible. In all cases the drop height was 11 cm and the plane was inclined at an angle of 5° 45' with the horizontal. Settled bed depths were held at approximately 35 cm. Flow distances for both fluidized and unfluidized materials are reported. Again the F-2-25 catalyst exhibited the best flow properties, followed, in this case, by the FCCU catalyst and then the ash-flow tuff. Some indications of the effect of the particle size on flow properties may be obtained from an analysis of the granite data. Here a decrease in particle size results in an increase in distance traveled. Glass microspheres show a similar trend. Although no narrow cuts were investigated in the case of ash-flow tuff, the importance of the smaller particles in determining the flow properties of the material is obvious. In both samples shown in Table XXIII, the larger particles appear to have little effect other than to prevent agglomeration of the smaller particles. Flow properties are determined primarily by the smaller particles.

Table XXIII

FLOW PROPERTIES OF FLUIDIZED MATERIALS

Drop height 11 cm Plane Angle 5°45'

Material	Size, microns	Settling Rate, cm/sec	Depth of Bed, cm		Expansion Ratio	Spread, cm	
			settled	expanded		down plane	across plane
FCCU	> 37	0.65	34.5	42.5	1.23	82	79
	> 37		35.6	-		30	29
Talc	53-10	1.6	36.0	51.0	1.42	52	42
	53-10		34.0	-		30	30
Granite	177-149	1.8	34.5	40.0	1.16	30	29
	177-149		34.5	-		28	28
Granite	88-74	1.8	34.5	42.0	1.22	34	34
	88-74		34.5	-		22	23
Granite	< 44	2.2	33.2	40.0	1.20	38	39
	< 44		33.0			26	29
Glass Beads	125-105	1.75	35.5	40.0	1.12	52	52
	125-105		35.5	-		44	43
Glass Beads	88-74	1.2	36.0	42.0	1.16	59	58
	88-74		36.0	-		46	44
F-2-25	105-20	0.55	34.5	49.0	1.42	120+ (1)	87+ (1)
	105-20		34.5	-		26	26
Ash-Flow Tuff	< 125	0.73	34.5	49.5	1.44	69	72
	< 125		34.5	-		22	21
Ash-Flow Tuff	< 297	0.87	35.5	47.8	1.35	75	69
			35.5	-		23	24

(1) Material traveled maximum dimensions of tray

Some typical flow patterns for both fluidized and unfluidized materials are shown in Fig. 21 through 24. The effect of fluidization on the flow properties of the materials is obvious. Apparent discrepancies between photographs and data recorded in Table XXIII are due to variations in drop height or in the amount of material used in the test. An increase in either of these parameters results in an increase in the size of the flow pattern. The effect of drop height can be seen in the series of photographs in Fig. 24. The first photograph (a) shows the flow pattern resulting from unfluidized granite (-325 mesh) being dropped from a height of 11 cm. The second photograph (b) shows the flow pattern of this same material when fluidized. Again the drop height was 11 cm. In the third photograph (c), the same material was dropped from a height of 20.5 cm. The increase in the size of the flow pattern with increasing drop height is apparent. Fig. 25 and 26 were obtained using a column with a hole in the side near the bottom. Instead of removing the fluidizer and allowing the fluidized material to fall onto the plane, the fluidized material was allowed to flow from the side hole. The center of this hole was 6 cm above the level of the plane. Both flow velocity and distance traveled were determined. Again, the F-2-25 catalyst exhibited the better flow properties. This material had a flow velocity of 160 cm/sec and traveled the entire length of the plane (120 cm), while the ash-flow tuff had a flow velocity of only 80 cm/sec and traveled only 90 cm. These results are in general agreement with flow velocities and travel distances reported earlier.

Since the distance traveled by the particles under a standard set of conditions is the most important factor in choosing a material for large-scale demonstration, it was wondered if there were any relationship of properties which could be used to predict the results. Table XXIV lists the materials in decreasing order of distance traveled. The settling rate appears to give a good general idea, with the lowest rate permitting the greatest travel distance. Horizontal flow velocities were not as meaningful. However, it has been found that the expansion ratio divided by the particle density and settling rate gives a better correlation. Values are shown in Table XXIV and plotted in Fig. 27. It is not known whether this relationship has any theoretical justification, but it is interesting to note the dimensional relationship in the plot of distance traveled vs $\frac{\text{Expansion Ratio}}{(\text{density})(\text{settling rate})}$

$$\text{cm} \quad \text{vs} \quad \frac{1}{(\text{g/cm}^3)(\text{cm/sec})}$$

$$\text{cm} \quad \text{vs} \quad \frac{\text{cm}^2\,\text{sec}}{\text{g}}$$

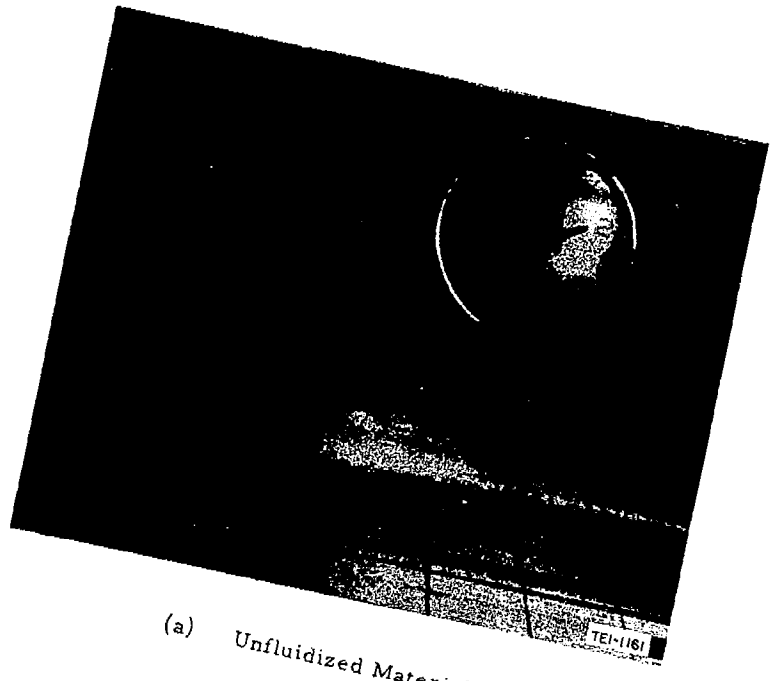

(a) Unfluidized Material

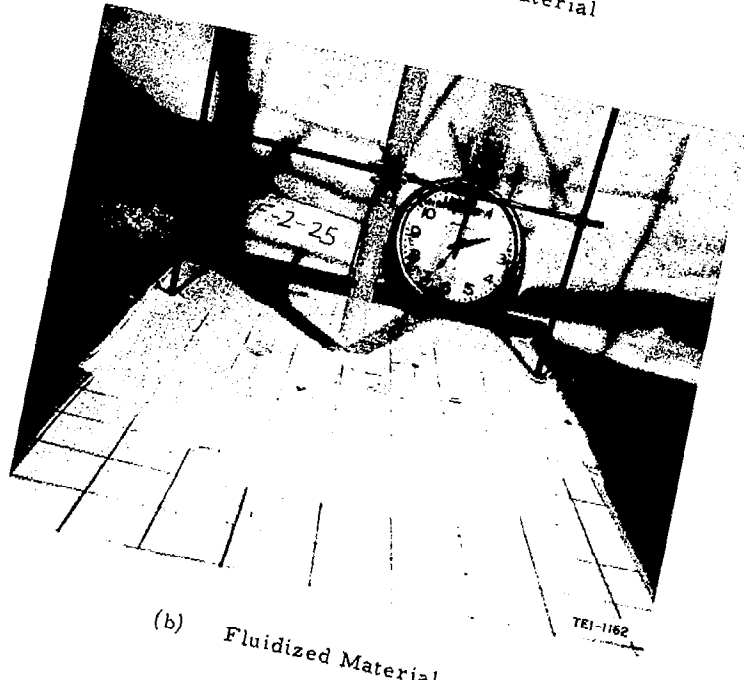

(b) Fluidized Material

Fig. 21 Flow Pattern of F-2-25 Catalyst (Unsized, 5-cm Drop Height)

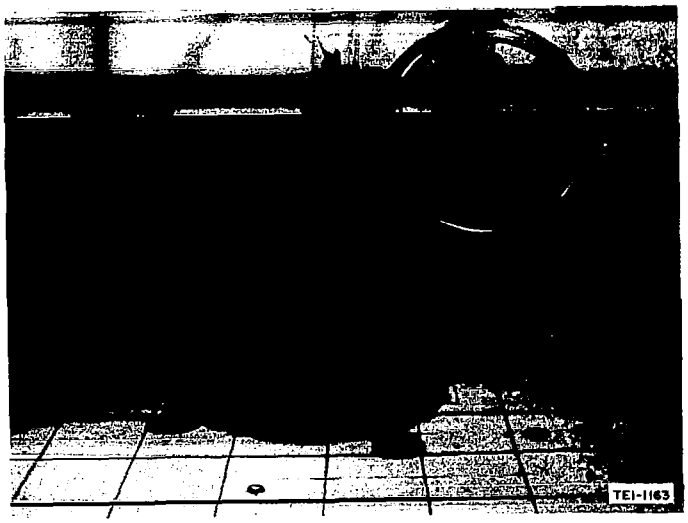

(a) Unfluidized Material

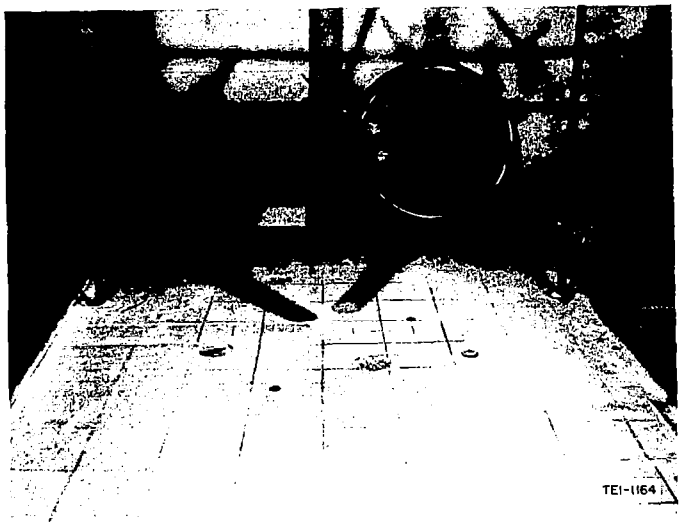

(b) Fluidized Material

Fig. 22 Flow Pattern of Unwelded Ash Flow Tuff (All Particles Less Than 125 μ, 11-cm Drop Height)

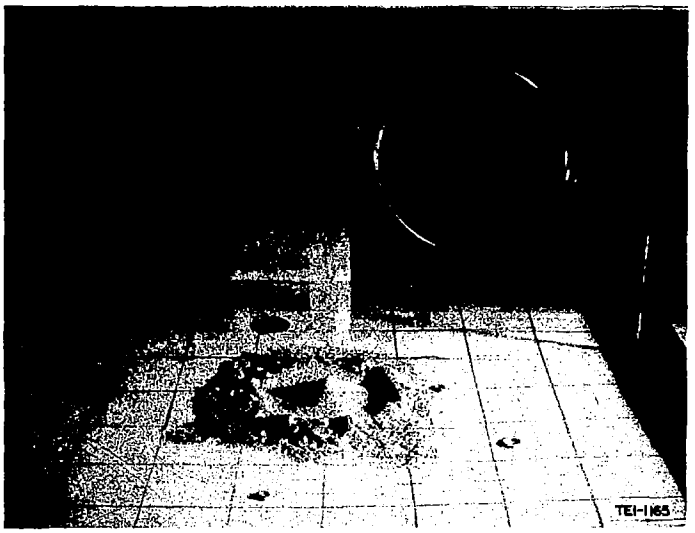

(a) Unfluidized Material

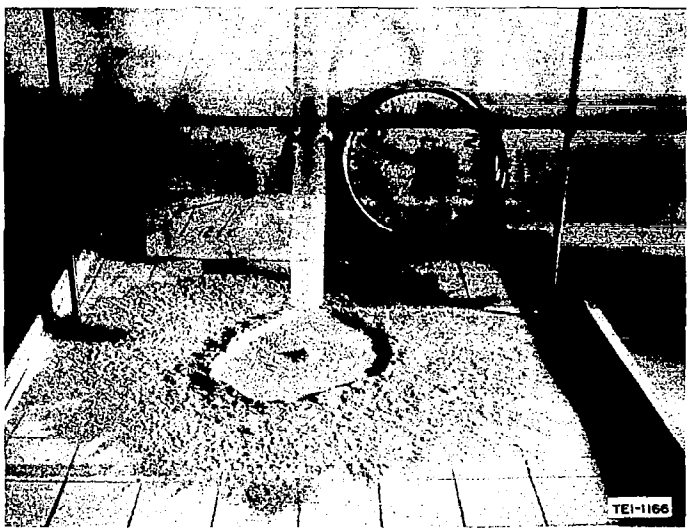

(b) Fluidized Material

Fig. 23 Flow Pattern of No. 325 Talc (Unsized, 11-cm Drop Height)

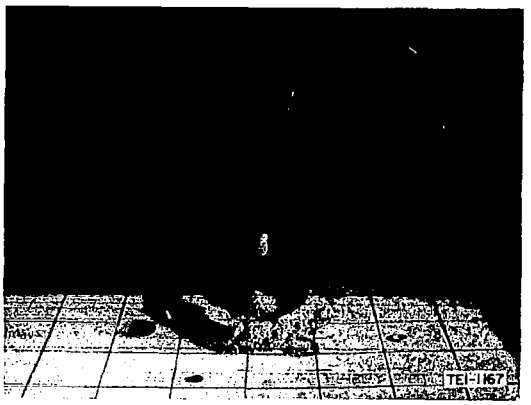

(a) Unfluidized Material

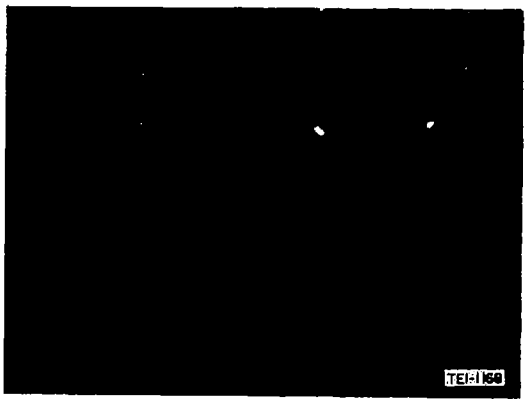

(b) Fluidized Material

(c) Fluidized Material (20.5-cm Drop Height)

Fig. 24 Flow Pattern of Crushed Granite (Particles Less Than 44 μ, 325 Mesh, 11-cm Drop Height)

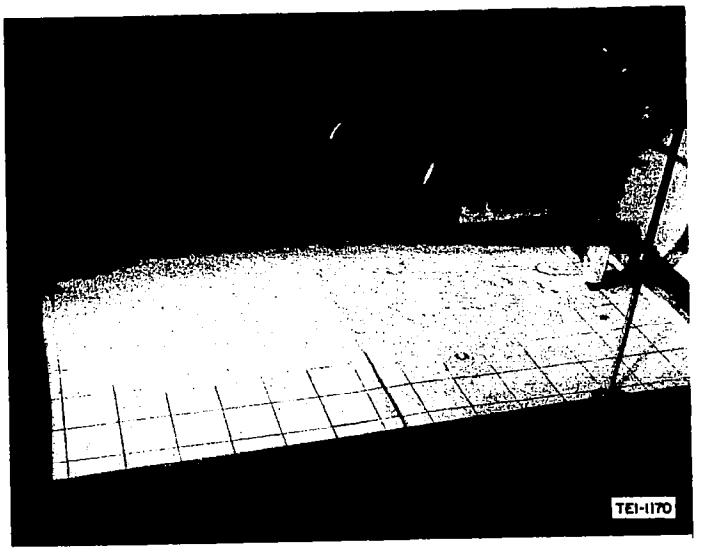

Fig. 25 Flow Pattern of F-2-25 Catalyst - Side Ejection

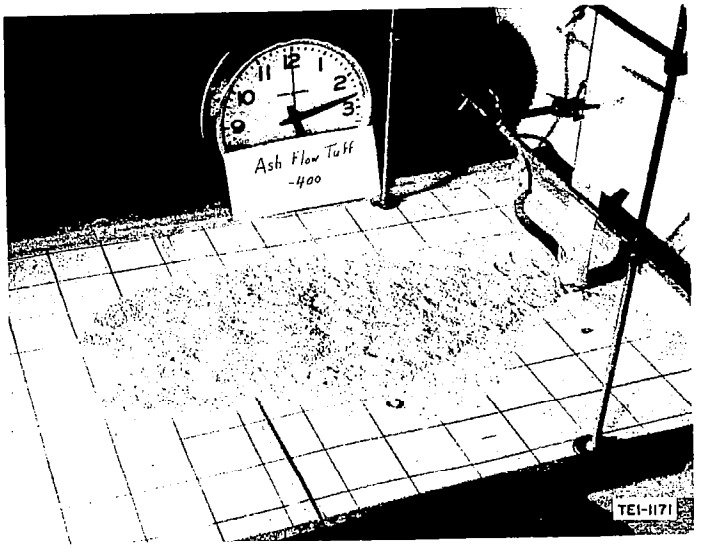

Fig. 26 Flow Pattern of Unwelded Ash Flow Tuff - Side Ejection

Table XXIV

FACTORS AFFECTING DISTANCE TRAVELED

Material	Size Microns	Distance Traveled cm	E Expansion Ratio	S Settling Rate cm/sec	ρ Particle Density g/cm^3	$\frac{E}{\rho S}$
F-2-25	105-20	120+	1.42	0.55	0.767	3.36
FCCU	< 37	82	1.23	0.65	1.455	1.30
AFT	< 125	69-72	1.44	0.73	2.154	0.92
	< 297	69-75	1.35	0.87	2.154	0.72
Glass	88-74	59	1.16	1.2	2.48	0.39
	125-105	52	1.12	1.75	2.48	0.26
Talc	53-10	52	1.42	1.6	2.83	0.314
Granite	< 44	38	1.2	2.2	2.57	0.213
	88-74	34	1.22	1.8	2.57	0.26
	177-149	30	1.16	1.8	2.57	0.25

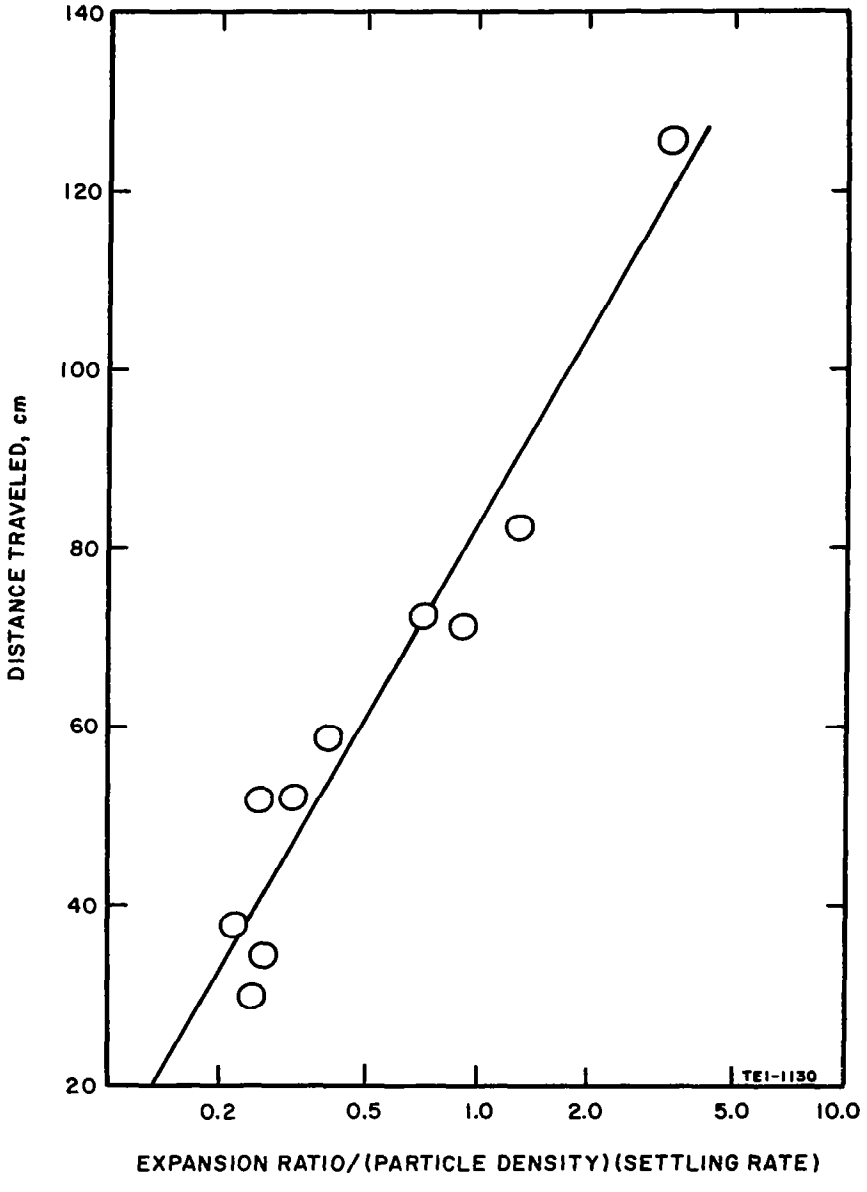

Fig. 27 Effect of Expansion Ratio, Particle Density and Settling Rate on Travel Distance

or in dimensional analysis $\ell \sim \ell^2 \, t \, m^{-1}$

$\ell \sim \ell \, (\ell \, t \, m^{-1})$

The dimensions $\ell \, t \, m^{-1}$ are those of fluidity.

Thus $\ell \sim \ell$ (units of fluidity)

3. Particle Separation

During the determination of the flow properties of the unwelded ash-flow tuff (smaller than 297 microns), it was noticed that particle fractionation of some sort was occurring in the fluidization column. This may be seen in Fig. 28, where there is a distinct band of material differing in color and texture from the rest of the samples. Attempts to remove the material for examination were not successful because remixing could not be avoided. However, examination of larger particle size material (590 to 840 micron) under a binocular microscope showed a variety of particles, some porous and some nonporous. This is illustrated in the previously discussed Fig. 8. The material could be separated by tweezers and the densities of the different types of particles could be measured.

The nonporous material, which resembles the band of material separated in the fluidization column, had densities in the range of 2.37 to 2.55 g/cm^3. The porous material, which is similar to the upper material in the column, had an average density of 1.43 g/cm^3. It is believed that the separation observed in Fig. 28 represents a density fractionation with the harder, nonporous, non-vesiculated material being concentrated toward the bottom of the fluidization column.

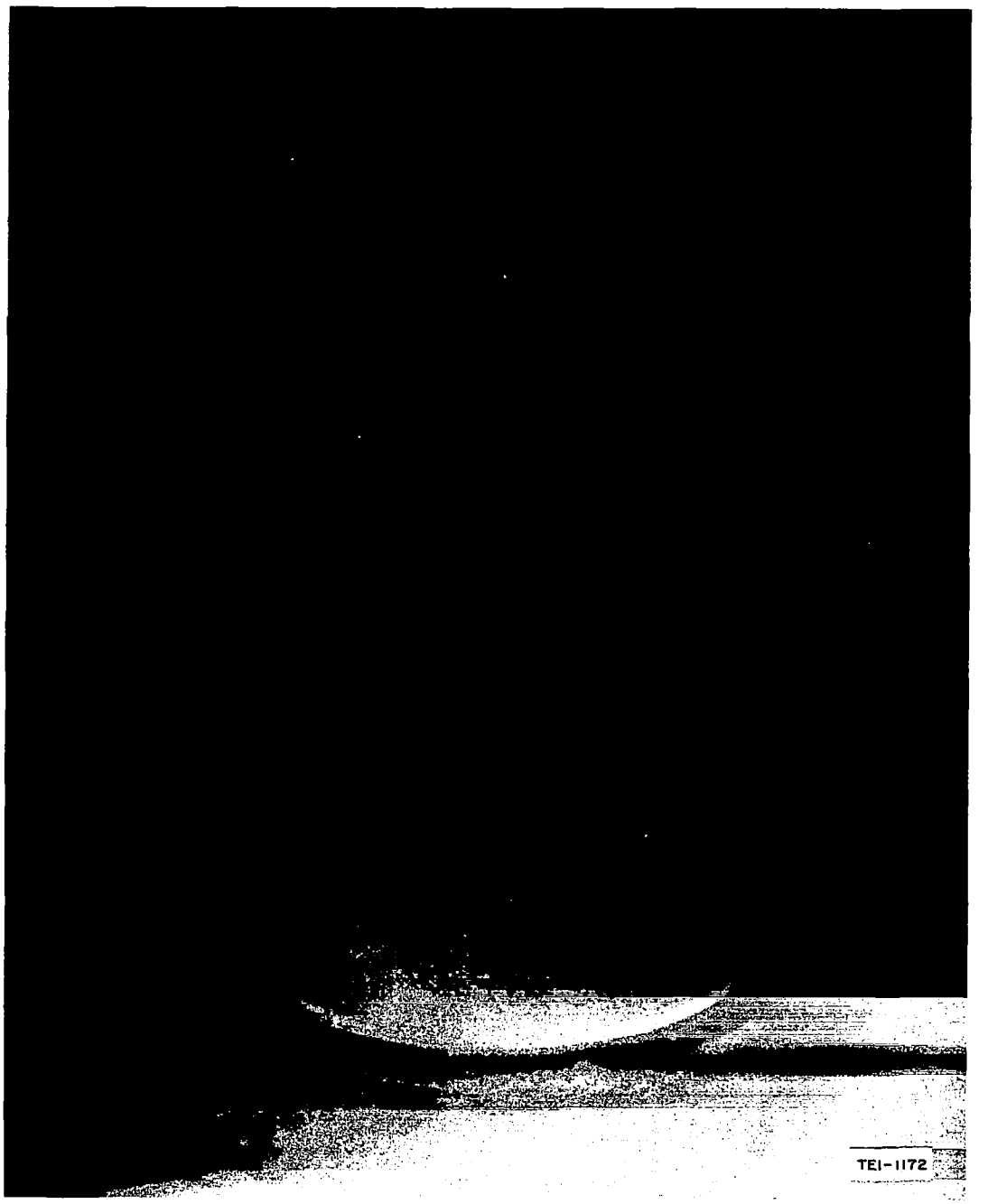

Fig. 28 Particle Fractionation Resulting From Fluidization of Ash Flow Tuff (Smaller Than 297 Microns)

D. VACUUM FLUIDIZATION

In any study of lunar fluidized-ash flow, one of the chief technical questions to be considered is the effect of vacuum on the fluidization process. For example, what happens in a fluidized column when the pressure above the column is reduced to the point where Poiseuille's law is no longer operative? Is it still possible to obtain uniform fluidization under these conditions? If so, how far below the surface is the column affected by a reduction in pressure above the column?

In an attempt to answer such questions as these, the vacuum fluidization system shown in Fig. 29 was constructed. The system was designed to operate over a pressure range from 0.3 torr to 1.0 atmosphere with special emphasis on the lower pressures. Of primary importance was that region where the mean free path of the gas approximated the particle diameter. In the present investigation, this was in the vicinity of 2 torr. At this pressure and room temperature, the mean free path of nitrogen molecules used as the fluidizing gas was approximately 35 microns. This is comparable to the size of the particles used in most of the low pressure studies. A plot of the mean free path of nitrogen molecules as a function of pressure is shown in Fig. 30.

The system was similar in many respects to the system used in studies at atmospheric pressure. Additional pressure gauges were installed at various points in the system to monitor pressure, and a high capacity vacuum pump (Kinny, Model KD30) was used to control the pressure. The vacuum system was connected to the fluidization column through a large (250 liter) buffer tank. The purpose of the tank was to smooth out any fluctuations in column pressure originating in the vacuum pump. Pressure in the column was controlled by means of a vacuum valve located between the pump and the buffer tank. A filter unit, installed just ahead of the buffer tank, prevented excessive amounts of elutriated material from entering the pump. Gas pressure above the bed was measured on a Dubrovin gauge covering a range 0 to 20 torr and capable of being read accurately to 0.1 torr. Fluidizing gas flows were controlled by sonic-orifice flowmeters.

Although a number of different materials were investigated under near vacuum conditions, a majority of the results were obtained with FCCU catalyst primarily because of the smoother and more consistent behavior of this material. All materials tested showed the same general behavior. The F-2-25 catalyst was quite difficult to fluidize at pressures below about 10 torr and elutriation of this material was quite bad. While operating at a

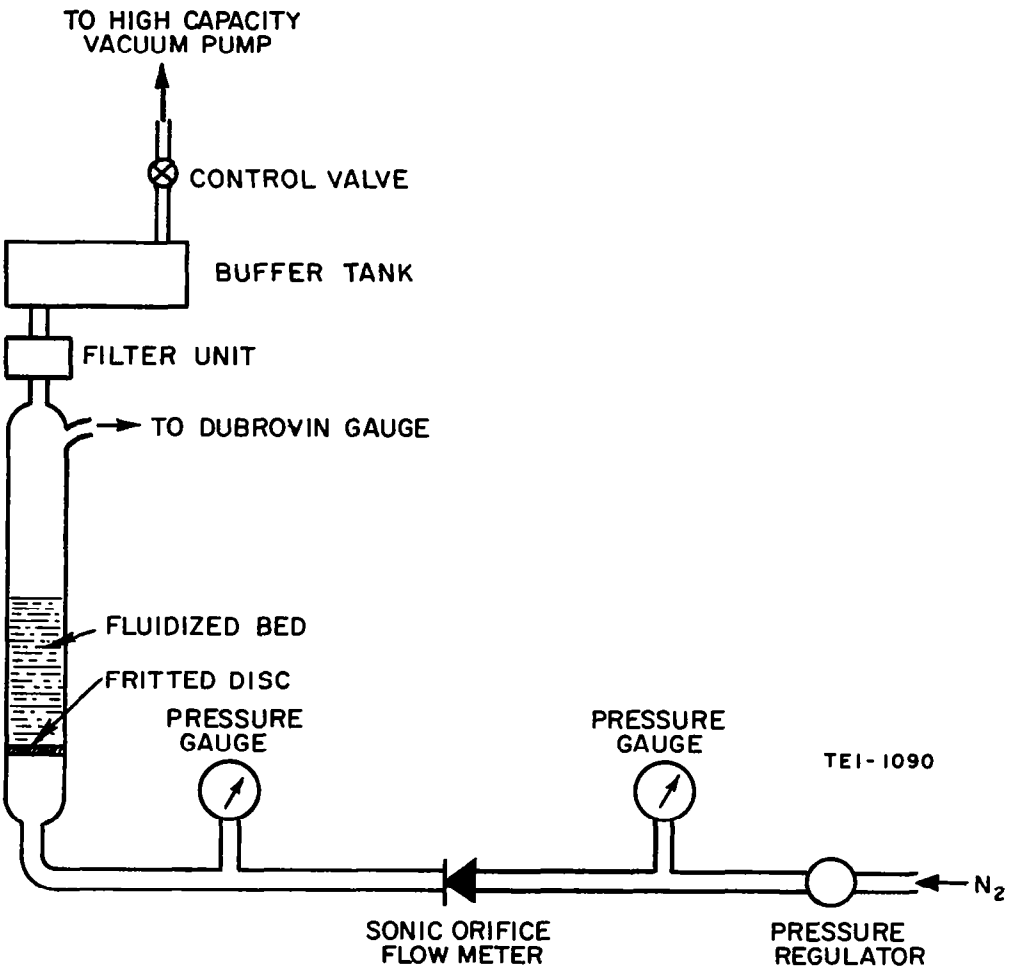

Fig. 29 Low Pressure Fluidization System

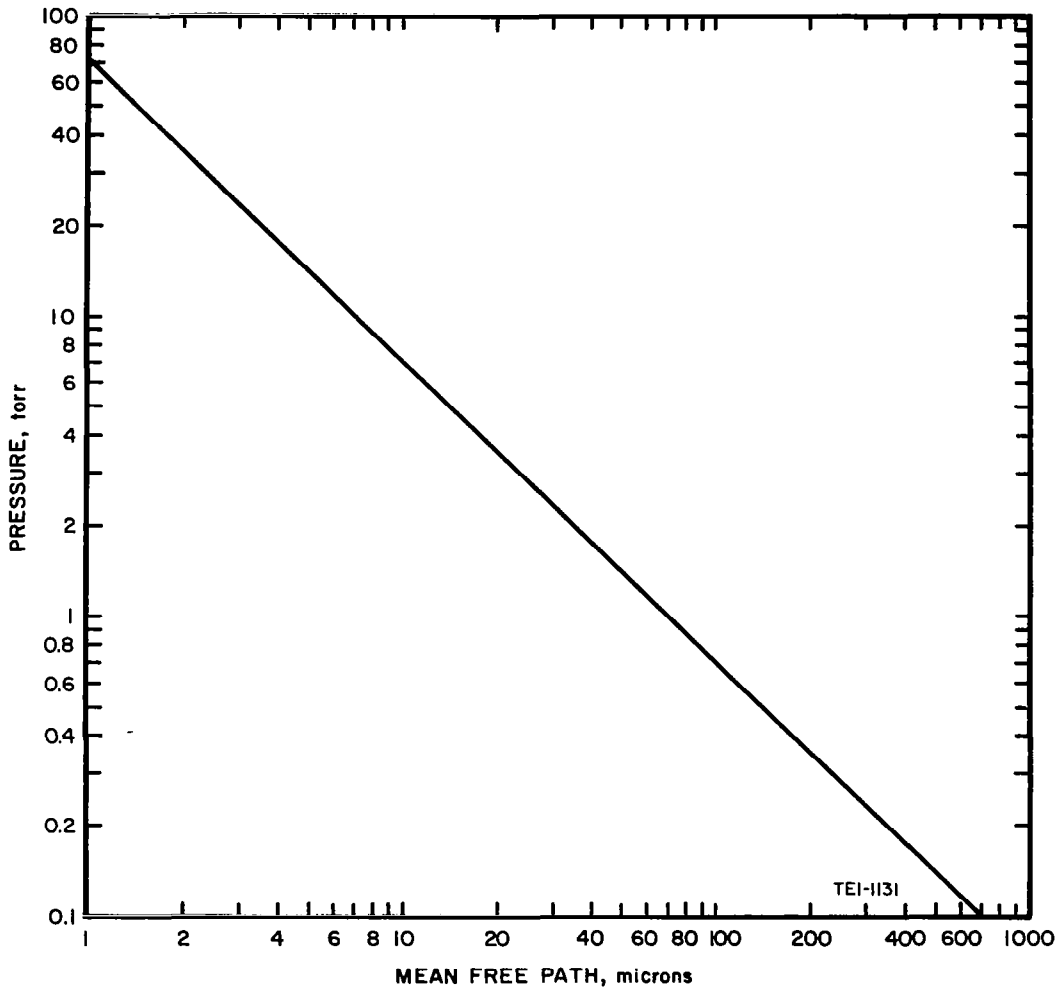

Fig. 30 Mean Free Path of Nitrogen Molecules as a Function of Pressure

pressure of 2 torr, using particles 37 microns and less in diameter, approximately 35 cc of material was lost by elutriation in 30 minutes. Ash-flow tuff of similar size was equally as difficult to fluidize. No uniform fluidization could be obtained under any conditions with this material at pressures below about 5 torr. Elutriation was about the same as with the F-2-25 catalyst.

Glass beads (No. 4000) had some tendency to agglomerate but could be fluidized at pressures as low as 0.4 torr provided the column of material was not too deep. Increasing the depth of bed material tended to reduce the amount of expansion of the column and made fluidization more difficult.

This effect of bed depth was also observed with unsized FCCU catalyst where an increase from 10 to 22.6 cm decreased the maximum expansion ratio of the bed from 1.16 to 1.04 at a pressure of 0.7 to 0.9 torr. Results with 37 to 53 micron FCCU catalyst show that, for a given bed depth, the expansion ratio of the bed was quite sensitive to changes in pressure at the surface of the bed, particularly in the pressure range where Poiseuille's law begins to fail. This is shown graphically in Fig. 31 (data, in addition to the two points discussed above, are from Tables XXV and XXVII) where expansion ratio is plotted as a function of pressure for different bed depths. At the lower pressures - below about 1 torr, practically no expansion of the column occurs. Further increase in gas flow resulted in rather violent agitation or slugging of the column but no increase in expansion.

A cross plot, taken from smoothed data of previous Fig. 31, of expansion ratio versus bed depth at 1 torr is shown in Fig. 32. This demonstrates that even with the FCCU catalyst, (which was more smoothly fluidized at very low pressures than any of the other materials), there is a limit to the bed depth at which fluidization can occur. The expansion ratio appears to approach unity (no expansion) at a bed depth between 40 and 50 cm.

Referring again to Fig. 31, as the pressure was increased, expansion of the column increased although it was still not possible to obtain uniform or steady fluidization. For the size particles used in these runs, the critical pressure - where the mean free path in the gas equals the particle diameter - is about 2 torr. At pressures greater than this, the expansion ratio of the bed begins to increase rather rapidly.

In the vicinity of this "critical pressure", with proper adjustments of flow and pressure, it is possible to obtain stable, uniform fluidization of the bed for a limited time. This is shown in Fig. 33 where the top of the fluidized bed is relatively stable. Some powder sticks to the wall, partially obscuring the view of the top surface. This stable fluidization lasts for

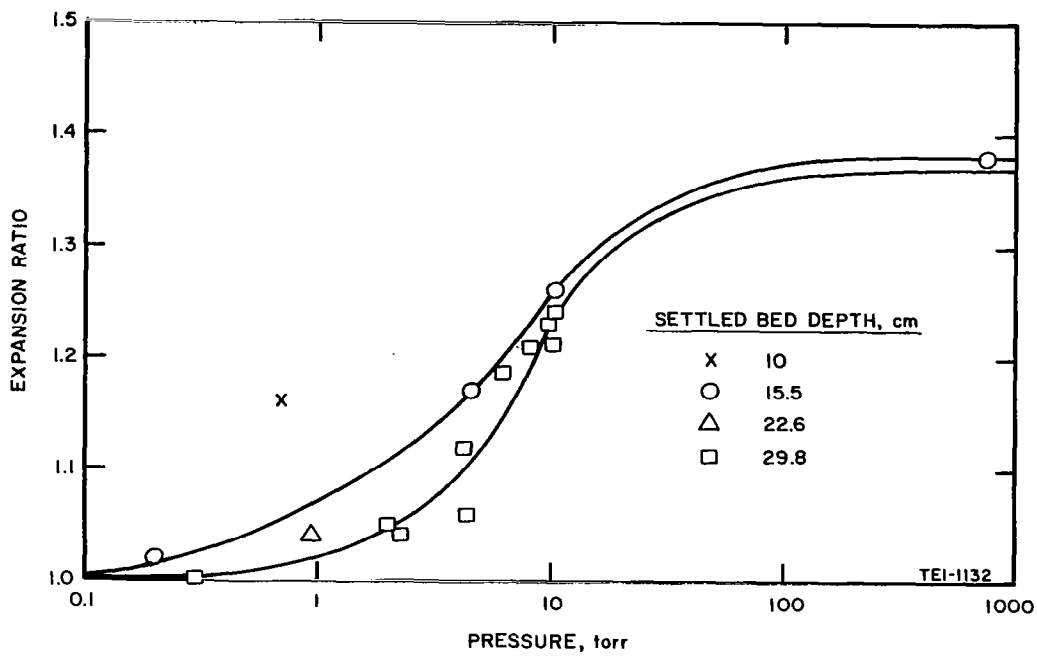

Fig. 31 Effect of Vacuum on Expansion Ratio of FCCU Catalyst

Table XXV

Summary of Low-Pressure Fluidization Data of 37-53 micron FCCU catalyst at a Settled Bed Depth of 15.5 cm

$P_{(\text{above bed})}$, mm Hg	4.4	10.1
$\Delta P_{(\text{bed + disc})}$, cm Hg	1.1	1.2
Flow, cm^3/sec	0.24	0.35
Fluidization	smooth	smooth
Expanded ht., cm	18.1	19.5
Expansion ratio	1.17	1.26
ΔP/cm of expansion ht.	0.061	0.061

Comparison of pressure drop across bed and pressure due to weight of bed.

Pressure drop = 1.1 cm Hg = $\underline{14.9\ gm/cm^2}$

Pressure due to weight of column:

$(0.83\ gm/cm^3)\ (15.5\ cm) = 12.9\ gm/cm^2$

The pressure drop slightly exceeds the weight of bed material. Agreement is reasonably good and difference is probably due to pressure drop across disc.

Table XXVI

Summary of Low-Pressure Fluidization Data of 37-53 micron FCCU catalyst at a Settled Bed Depth of 28.9 cm

$P_{(\text{above bed}),}$ mm Hg	0.5	2.2	10.2
$\Delta P_{(\text{bed + disc}),}$ cm Hg	1.6	2.1	2.4 **
Flow, cm^3/sec	0.137	0.215	0.39
Fluidization	no expansion *	burping	smooth
Expanded ht., cm	29.8	31.5	36.0
Expansion ratio	1.03	1.09	1.25
ΔP/cm of expansion ht.	0.054	0.067	0.067

Comparison of pressure drop across bed and pressure due to weight of bed.

Pressure drop of 1.6 cm Hg = 21.7 gm/cm^2 ***

Pressure due to weight of column: (.83 gm/cm^3) (28.9 cm) = 24 gm/cm^2

Pressure drop of 2.1 cm Hg = 28.5 gm/cm^2 ****

---

* Under these conditions the bed expanded less than 1.0 cm. Any increase in flow caused considerable burping of the column but no increase in expansion.

** Increase in pressure drop here is probably due to pressure drop across disc. Flow is higher here than in other runs. Similar result was observed in earlier runs.

*** Pressure drop is slightly below weight of material. Conditions for fluidization are not met. Column showed no appreciable expansion. However, a slight increase in flow (or back pressure) caused burping.

**** This is slightly in excess of the weight of bed material.

Table XXVII

Summary of Low-Pressure Fluidization Data of 37-53 micron FCCU catalyst at a Settled Bed Depth of 29.8 cm

$P_{(\text{above bed}),\ \text{mm Hg}}$	2.2	2.0	4.4	4.2	9.8	6.1	9.8	8.0
$\Delta P_{(\text{bed + disc}),\ \text{cm Hg}}$	1.8	2.1	2.0	2.2	2.0	2.1	2.2	2.3
Flow, cm^3/sec	0.192	0.190	0.206	0.24	0.326	0.31	0.345	0.333
Fluidization	burping	burping	smooth	smooth	smooth	smooth	smooth	smooth
Expansion Ht., cm	31.0	31.4	31.7	33.5	36.0	35.4	36.7	36.2
Expansion ratio,	1.04	1.05	1.06	1.12	1.21	1.185	1.23	1.21
ΔP /cm of expansion ht.	0.058	0.067	0.063	0.066	0.056	0.059	0.060	0.064

Comparison of pressure drop across bed and pressure due to weight of bed.

Pressure drop at 1.8 cm Hg = 24.4 gm/cm^2

Pressure drop (average) = 2.1 cm Hg = 28.5 gm/cm^2

Pressure due to weight of column: (0.83 gm/cm^3) (29.8 cm) = 25 gm/cm^2

The first ΔP of 1.8 cm Hg is below weight of column and conditions for fluidization are not met.

For average value of ΔP = 2.1 cm Hg or 28.5 gm/cm^2, this is slightly in excess of weight of bed material and the bed should be fluidized.

With flow adjusted to give maximum expansion:

$P_{(\text{above bed}),\ \text{mm Hg}}$	10.6
$\Delta P_{(\text{bed + disc}),\ \text{cm Hg}}$	2.2
Flow, cm^3/sec	0.36
Expansion ht., cm	37.
Expansion ratio	1.24
ΔP /cm of expansion ht.	0.060

Under these conditions, the bed expanded to 37 cm and remained at this height for approximately 60 seconds. During this time the bed was quite stable. After about 60 seconds, the bed became rather turbulent, and collapsed to a height of 30.2 cm. After settling, the bed would again slowly expand to a height of about 37 cm, stabilize for about 60 seconds, and then collapse again.

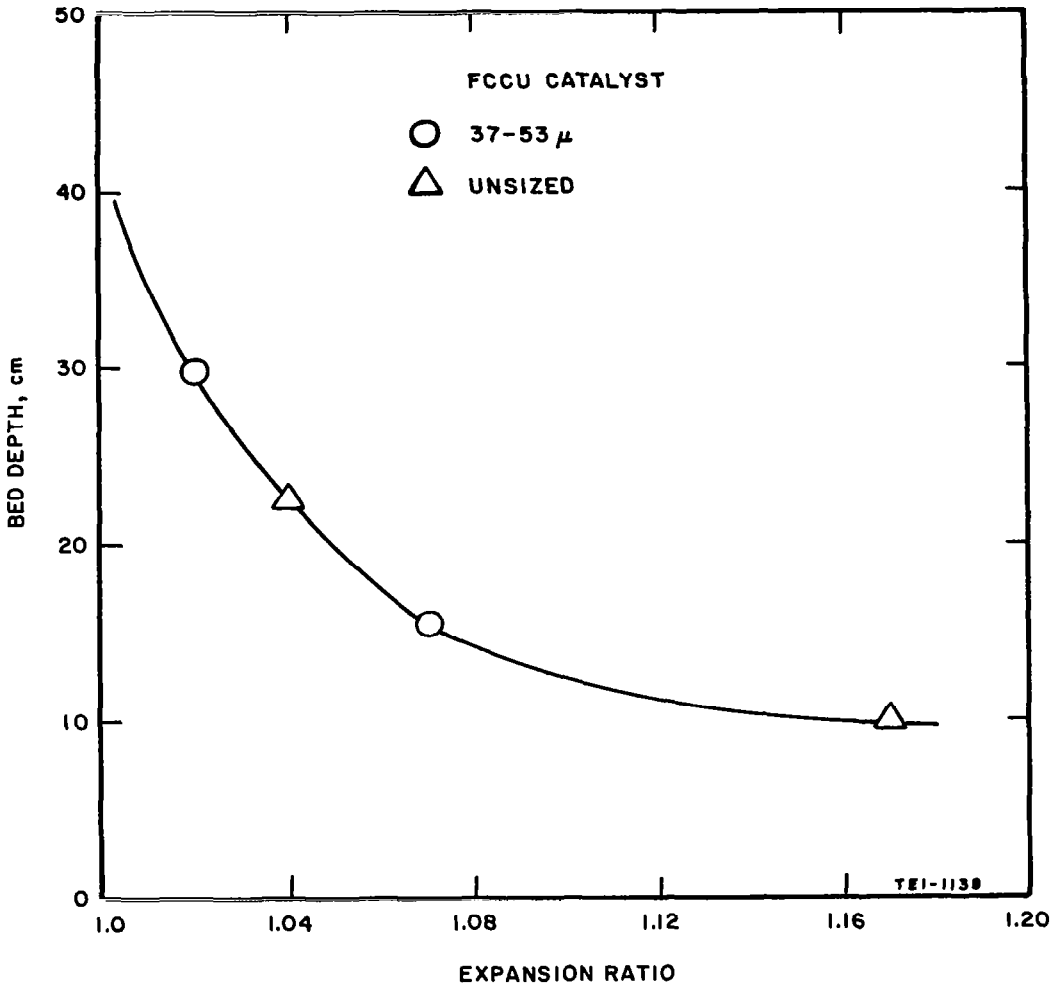

Fig. 32 Bed Expansion as a Function of Bed Depth at 1.0 Torr

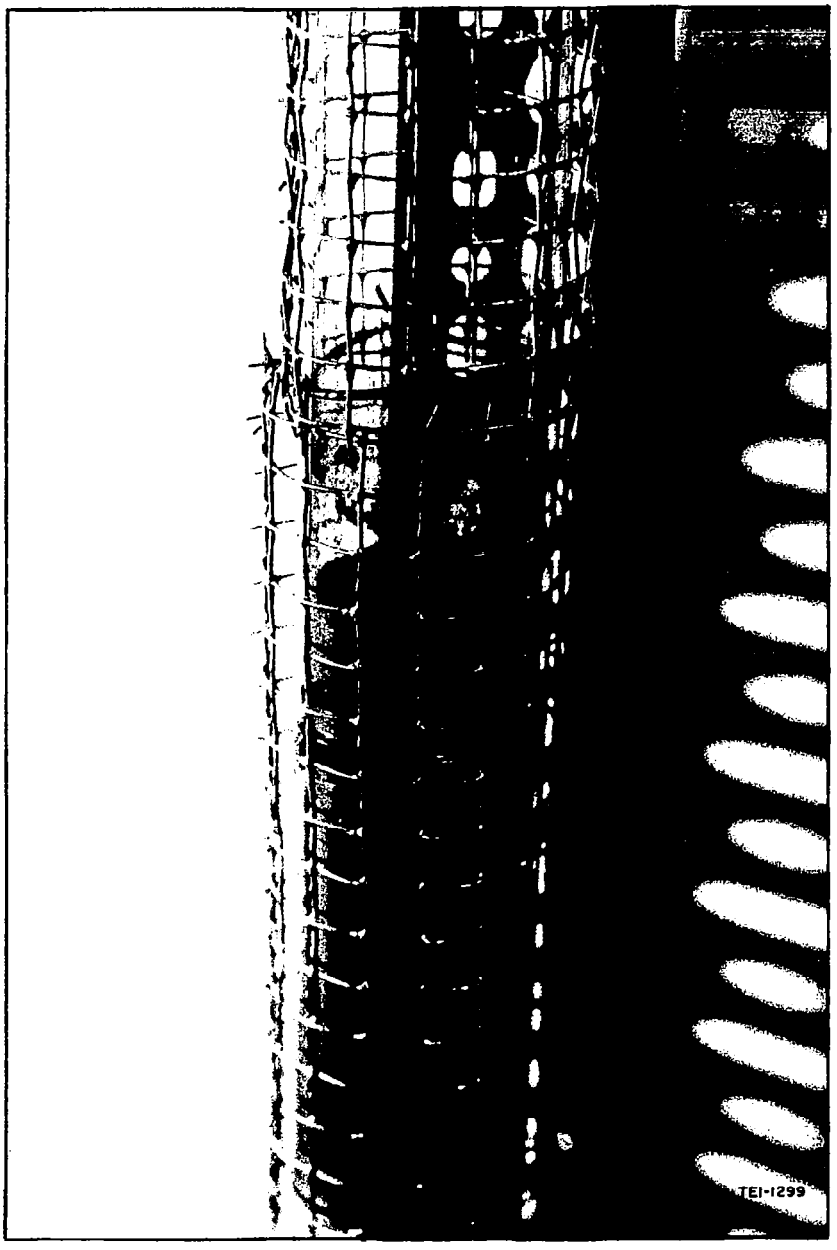

Fig. 33 Photograph of Stable Fluidization of FCCU Catalyst Under Vacuum Conditions

about 1 to 2 minutes. Then suddenly, the surface of the bed begins bubbling rather violently. Figure 34 was taken at an instant when the violent bubbling erupted and caused a rise of about 5.5 to 6 cm. After 10 to 15 seconds of bubbling, the surface calms down and the bed becomes stable for another 1 to 2 minutes, then the action is repeated. A similar action was observed in the case of glass microspheres. At pressures above about 5 torr---the exact pressure depends on the type of material being fluidized---the erratic behavior ceases and uniform fluidization of the column is achieved.

It is of interest in the case of a vacuum to estimate the depth below the surface of a fluidized bed where the pressure is above the critical so that Poiseuille's law can operate. Presumably, below this depth normal fluidization might take place. Pressure drop data through the bed were obtained in a series of vacuum runs for various pressures above the bed and for several depths of bed, using 37 to 53 μ FCCU particles. The results are shown in Tables XXV, XXVI, and XXVII.

The pressure drop, ΔP (bed + disc), represents the actual pressure drop across the bed and diffuser disc. It is the difference between the back pressure on the column and the pressure above the column. At the low flows used, the pressure drop through the disc was not measured but is relatively low. By comparing the ΔP (bed + disc) to the weight of the material in the column for all the runs, the ΔP (bed + disc) averages about 16 percent high. This is probably due to the pressure drop through the disc.

The data of Tables XXV through XXVII show the expanded height of the bed and the measured pressure drop ΔP (bed + disc). The average of all these values is 0.062 ΔP/cm of expanded bed height. Adjusting this value for the 16 percent pressure drop due to the disc, the approximate pressure drop is (0.062) (0.84) = 0.052 cm Hg/cm bed height.

For the 37 to 53 μ FCCU particles, the critical pressure where the mean free path of the gas is the same as the size of the smaller particles is about 1.5 to 2 torr. The bed depth from the top to give 2 torr (0.2 cm) is 0.2/0.052 = 3.85 cm. For smooth fluidization and moderate expansion of the bed, the pressure required is about 4 torr. This would require a depth from the top of 0.4/0.052 = 7.7 cm. These values must be used with caution since the 3.85 cm represents a hypothetical layer at the top of the column which would not be fluidized. If vapors continue to fluidize the lower part of the column, they must pass out through this hypothetical layer. The latter must be raised upward either in a burping action as was experimentally observed at the very low flows near the critical region or else blown violently upward into a dilute phase as was observed when

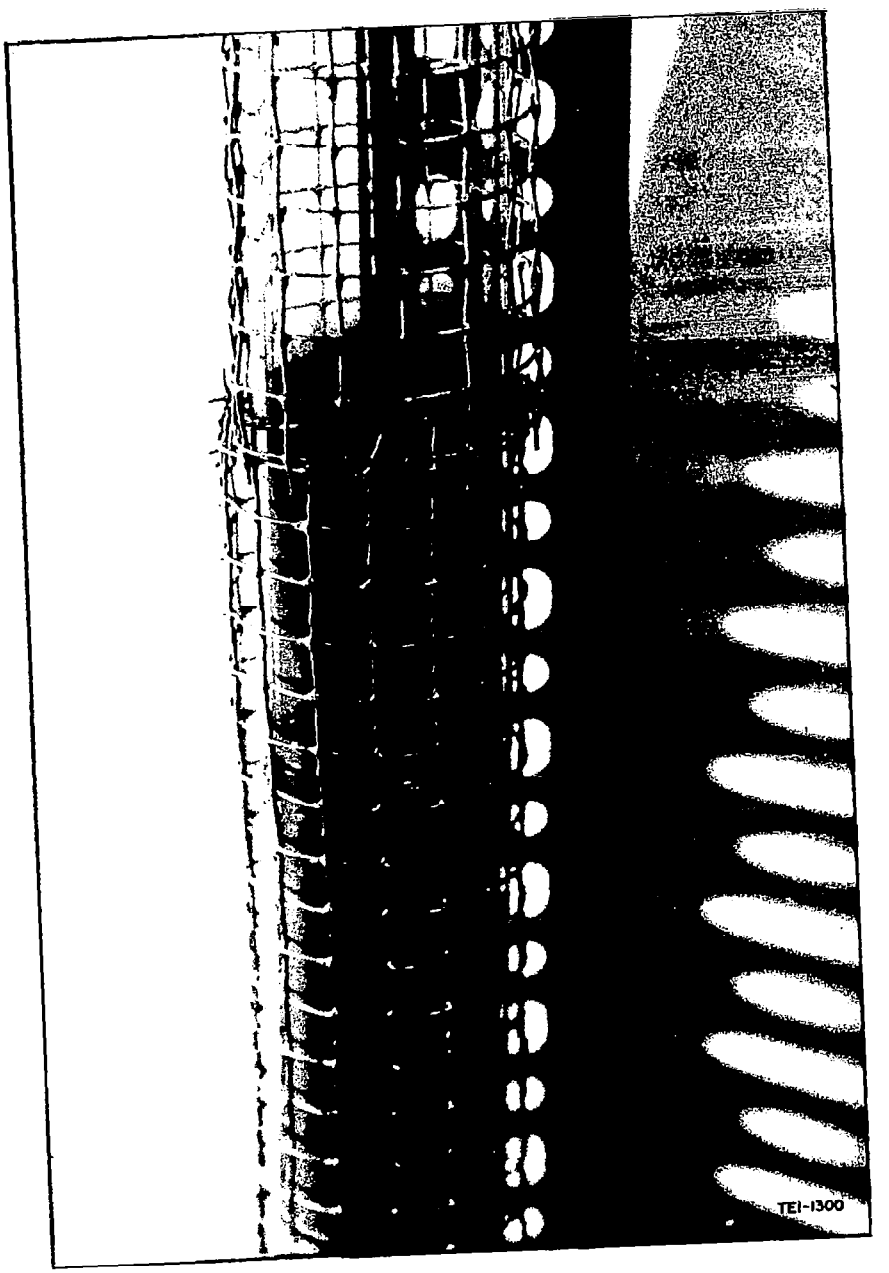

Fig. 34 Photograph of Erupting FCCU Catalyst Under Vacuum Conditions

appreciable elutriation took place at moderate flows. In a lunar eruption where large mass flows were taking place during all but the latter stages of the eruption, the top layer must be blown into an extensive dilute phase.

E. DISCUSSION OF RESULTS

Settling rates of fluidized particles could be measured with reasonable precision. They appear to be a strong indication of the distance a fluidized bed may travel horizontally after being released from the fluidizing column. The settling rates are independent of bed height but may be initially slightly high at very high bed expansions. Particle size has a definite effect on settling rate, the larger particles settling more rapidly. For narrow size cuts, they appear to follow the same slope relationship as predicted by Leva's equations for calculating minimum gas flow required for fluidization. That is, the settling rate for the larger particles appear to be proportional to the particle diameter to the 1.82 power. Smaller particles, however, diverge from this relationship and appear to settle faster than would be predicted. This is believed to be caused by small-particle agglomeration. On broad cuts, the settling rate increases as smaller particles are removed. However, large particles tend to prevent agglomeration of smaller particles and increase the effectiveness of small particles in controlling settling rate.

The expansion ratio is indicative of the void fraction of fluidized beds. The ratio increases for narrow cuts, as the particle size is reduced. Similarly, the expansion ratio for broad cuts increases with the proportion of small particles present. The expansion ratio, with the exception of talc, was greater for the lighter, more porous materials such as F-2-25 catalyst, ash flow tuff, and FCCU catalyst. Granite and glass microbeads were relatively low. The talc had a high ratio, presumably because of its flat-platelet particle shape.

The minimum gas flow, G_{mf}, for fluidization is well described by Leva's equation. This equation can be used to show the effect of different fluidizing gases or vapors and the effect of particle size and density. In comparing various size glass microspheres and ash-flow tuff, several things may be noted. The observed minimum gas flow for the glass beads was less than that calculated from the equation, while that observed for the ash flow was just slightly higher than that calculated. In addition, because of lower density, calculated gas required for ash flow appears less than for the glass spheres. Actually, the observed minimum gas flow for ash-flow tuff was 1.25 times that for the beads. This difference suggests that a suitable shape factor may be required. The usual shape factor, which is commonly employed in Stoke's low relationships, assumes unity for a sphere and below unity for all other shapes. This is the wrong direction for the observations made here, and the non-spherical particles require a factor greater than unity.

It should also be noted that the Leva equation works well for larger size particles, but below about 40 to 60 micron size particles, the fine material begins to show substantial deviation. This is believed caused by small particle agglomeration.

Flow velocities and horizontal flow distances were, of course, studied in the absence of gases emitted from the particles or without gases rising from below as would occur in a natural ash flow. Therefore, the values measured are low and are valid only for a comparison of the materials studied and as an indication of what to expect in a large-scale laboratory demonstration. The horizontal flow velocities were highest for F-2-25 catalyst, ash-flow tuff, and talc. In general, the smaller the particles the greater the velocity but this may be negated at very small size where agglomeration may take over.

The horizontal distance traveled was greatest for F-2-25 catalyst, FCCU catalyst, and ash-flow tuff. In general, decrease in particle size gave greater distance. Obviously, the height at which the particles were discharged above the surface (kinetic energy) was a major variable. A good first approximation of the distance a material will travel is given by the inverse of its settling rate. The best correlation, however, appears to be given by dividing the expansion ratio by the particle density and the settling rate.

In using the above information to choose a material for large-scale laboratory demonstration, it must be recognized that a number of factors were not or could not be readily studied. These include the previously mentioned lack of emitted steam or of vapors rising through the particle during horizontal flow and, in addition, the studies were not made on freshly fractured surfaces at high temperature as would be possible in the fine grinding process. Whether this latter factor of fresh surface would enhance steam retention at the particle surface and allow it to be emitted from the surface during the flow can not be easily determined. However, the experimental results obtained indicate clearly that a room temperature, large-scale demonstration can be made with available materials.

The best flow characteristics were possessed by the F-2-25 catalyst and this material is sufficiently similar in shape and porosity to an ash-flow tuff that it is the recommended material for a large scale demonstration. Such a demonstration could show the general principles involved in a dense-phase flow and could illustrate the formation of ghost craters. The effect of lunar hard vacuum to produce a dilute-phase cloud and final surface patterns of a completed eruption could not be simulated in large scale but some of these factors might be shown in special experiments.

The study of the vacuum effect on fluidization is the first work of this nature, so far as is known, which has been conducted. The work is quite interesting in that it bears out predictions made concerning the real effect of pressure below the "critical pressure" where the mean free path of the fluidizing gas is greater than the particle size. Under these conditions, fluidization does indeed become difficult and, at some point, ceases entirely.

Experiments at pressures just above and just below the critical point were possible only by reducing vapor flows to very low values. The corresponding expansion ratios were lower and at very low pressures approached unity, indication no fluidization. At higher gas rates, violent bubbling began.

F-2-25 catalyst was very difficult to fluidize below about 10 torr and at 2 torr (the critical pressure for 37 micron material), substantial elutriation resulted. The ash-flow tuff would give no uniform fluidization below 5 torr and also had high elutriation loss. Glass microspheres which were smooth, could be fluidized as low as 0.4 torr if the column height was small, but additional bed height made fluidization very difficult. The FCCU catalyst, 37 to 55 μ size, was the easiest to fluidize at low pressure, but at a pressure of 1 torr, increases in bed height decreased expansion ratio so that it approached unity somewhere between 40 and 50 cm of bed. This may indicate a maximum bed height for vacuum fluidization in the critical region.

The FCCU catalyst did maintain smooth fluidization at 2.2 torr for 1 to 2 minutes followed by 10 to 15 seconds eruptions where material was thrown up from the surface to a height of 5.5 to 6 cm. The system then became quiescent and the cycle was repeated. At higher vapor rates, violent bubbling with considerable dilute phase and elutriation would result. However, above 4 to 5 torr, normal fluidization would occur.

It was found that the pressure drop through 3.85 cm of FCCU bed would equal 0.2 cm (2 torr) and, through 7.7 cm, would equal 0.4 cm (4 torr). Somewhere between these values the critical pressure would be exceeded so that a hypothetical layer about 4 to 8 cm thick would not be fluidized while at all lower depths, fluidization could occur. Actually, of course, the mass flow of gases fluidizing the low portions of the bed would continue to rise. Because of the reducing pressure above, the gases would expand and the gas velocity would be increasing. Finally when the gas reached the hypothetical unfluidized layer, this material would be blown upward to form a dilute phase or cloud. The extension of this description to a lunar ash flow will be obvious.

III. CONCLUSIONS

1. The fluidization properties of a number of materials could be rated so that the best material for a large scale demonstration of fluidized-ash flow could be made in the laboratory.

2. F-2-25 catalyst had the best fluidized properties judged by: a) flowing the greatest distance, b) having the highest travel velocity, and c) having the slowest settling rate after fluidization vapor is cut off.

3. Settling rate is independent of bed height but is affected by particle size and size distribution. The rate decreases with particle size but below 40 to 60 micron size, does not decrease as rapidly because of small particle agglomeration. On broad cut materials, the settling rate increases as smaller particles are removed; the presence of large particles tend to prevent agglomeration of smaller particles and enable the latter to control the settling rate.

4. Horizontal flow distance increases with smaller particle size but this may be negated at very small size (20 microns or less) where excessive agglomeration may take place. The flow distance correlates well with the factor of expansion ratio divided by particle density and settling rate.

5. Full range material such as the 20 to 105 micron size of F-2-25 catalyst is satisfactory for flow and no separation or grinding appears necessary.

6. Fluidization is affected by low pressure in the range where the mean free path of the vapor becomes larger than the particle dimensions.

7. For fluidization of 37 to 53 micron FCCU catalyst at a pressure of 2 torr, the maximum gas flow through the bed without violet bubbling is about 1.27×10^{-5} g/cm^2 sec. This is 10 to 20 times less than the minimum gas flow for fluidization at 1 atmosphere.

8. The hypothetical distance below the surface where fluidization can still occur in a vacuum is between 3.85 and 7.7 cm for the FCCU catalyst, based on pressure drop determinations.

9. Bed expansion ratio is decreased as pressure is lowered near the critical point and approaches unity (no expansion) rapidly below 1 torr.

10. Bed expansion ratio for FCCU catalyst is decreased as the bed height is increased. It approaches unity between 40 to 50 cm of bed height.

11. In a fluidized system of major dimensions, the effect of vacuum will be to cause the top surface to erupt into a dilute phase and to cause extensive elutriation.

IV. RECOMMENDATIONS

It is recommended that the F-2-25 catalyst be used for a large scale demonstration of fluidized ash flow and that recognition be given to the effect that vacuum has had on the mechanism of a lunar ash flow. The significance of the vacuum effect is that, in addition to possible dense phase flow, similar to terrestrial ash flows, lunar flows must have been accompanied by an extensive dilute phase wherein particles have been blown upward. These then must fall back to the surface near and immediately following the end of the eruption. Since these particles will remain very hot for long periods of time, and since the particle surfaces are newly formed and have not undergone reaction with an atmosphere such as on earth, there is a good probability of "vacuum" welding. The nature of the resultant surface can be studied experimentally and a suggested program is given in the following section.

V. FUTURE WORK

Results of the current program suggest additional studies which merit consideration. These include: 1) the large scale demonstration of fluidized ash flow; 2) the determination of the surface characteristics resulting from the settling back of the dilute-phase flow caused by the lunar vacuum; 3) measurement of the rock temperature and degree of vesiculation resulting from liberating water of crystallization from simulated lunar rocks; and 4) study of SiO_2 content enhancement which might result from sorting phenomena during fluidization (both elutriation sorting and density sorting were observed in this program).

The large scale demonstration could show all aspects of dense phase fluidized-ash flow and could be arranged to simulate dilute phase flow. It would illustrate the formation of ghost craters and should convincingly indicate the nature of the phenomenon by means of moving pictures. It can be carried out easily at room temperature using the F-2-25 catalyst. Because of the temperature and pressure, however, it will not indicate the probable final welded nature of the ash flow surface which can be better demonstrated as outlined in the next section.

It is felt that the dilute phase flow caused by the lunar vacuum will be very hot (about 850°C) and will cool only very slowly. Because particle surfaces are "clean", there will be a strong tendency to weld when the particles fall back to the lunar surface. It is suggested that this may be experimentally studied by observing the pattern obtained by dropping particles of unwelded ash-flow tuff onto a plane surface in a vacuum and then heating to red heat. The properties of the resultant vacuum-welded material can be determined. The measurement of the photometric response curve can also be carried out and compared to that obtained from the moon.

The temperature at which water is liberated from various rocks, and the degree of vesiculation can be measured to give a better understanding of this mechanism as it affects fluidization. Radio frequency heating of activated charcoal has been conducted here and the resultant liberation of adsorbed water has given an excellent simulation of fluidization. This RF technique (or ordinary conductive and convective heating) can be applied to water-bearing rocks such as serpentine. This will provide fluidization, permit temperature measurements to be made, and show the degree of particle fragmentation and vesiculation.

Silica concentration enhancement by fluidization may occur by the natural sorting which was observed in this program. If it can be shown that SiO_2 tends to concentrate, this may offer an explanation for the high SiO_2 content of tektites and glasses which have been hypothesized to have come from the moon. In fluidization, the more crushable and friable materials will produce smaller diameter particles and these will be preferentially carried upward and into the dilute phase. Additionally, material which contains less water and is less vesiculated as the result of an eruption will have fewer voids and a higher particle density. This material will be sorted from lesser density materials and tend to remain at lower portions of a fluidized zone. This could be experimentally studied by fluidization of an unwelded ash-flow tuff. Chemical analysis of sorted fractions resulting from elutriation and density fractionation should show the extent of SiO_2 concentration changes.

REFERENCES

1. Ralph B. Baldwin, "The Nature of the Lunar Surface and Major Structural Features", Proceedings of the Conference on Lunar Exploration, I, Paper VII, Bulletin of the Virginia Polytechnic Institute, Blacksburg, Va. LVI, No. 7, 1963.

2. H. C. Urey, The Planets, Yale University Press, New Haven, 1952.

3. T. Gold, Vistas in Astronautics: II Annual Astron. Symp., Pergamon Press, 1959, pp. 261-266.

4. E. M. Shoemaker and R. J. Hackman, "Procellarian System", Astrogeologic Studies, Semi-Annual Progress Report, U. S. Geological Survey, 1961, p. 2.

5. John A. O'Keefe and Winifred S. Cameron, "Evidence from the Moon's Surface Features for the Production of Lunar Granites", Icarus, 1, 1962, pp. 271-285.

6. John A. O'Keefe and Ernst W. Adams, "Tektite Structure and Lunar Ash Flows", Journal of Geophysical Research 70, 1965, pp. 3819-3829.

7. Clarence S. Ross and Robert L. Smith, "Ash-Flow Tuffs: Their Origin, Geologic Relations and Identification", Geological Survey Professional Paper 366, U. S. Govt. Printing Office, Washington, D. C., 1961.

8. C. N. Fenner, The Origin and Mode of Emplacement of the Great Tuff Deposit in the Valley of the Ten Thousand Smokes, National Geographic Soc. Contributed Technical Papers, Katmai serial no. 1, 1923, p. 72.

9. R. F. Griggs, The Valley of the Ten Thousand Smokes (Alaska), Washington, D. C. National Geographic Society, 1922, p. 253.

10. J. Westerveld, Geol. Soc. America Bull., 63, 1952, p. 561.

11. Abraham Dolgoff, The Volcanic Geology of the Pahranagat Range and Certain Adjacent Areas, Lincoln County, Southeastern Nevada, PhD Thesis, Rice Institute, Houston, Texas, 1960, p. 24.

12. F. R. Boyd, "Rhyolite Plateau, Yellowstone Park, Wyoming," Bulletin Geol. Soc. Am. 72, 1961, pp. 387-426.

13. N. A. Kozyrov, "Spectroscopic Proofs for Existence of Volcanic Processes on the Moon", The Moon, Ed. by Z. Kopal and Z. K. Mikhailov, Academic Press, N. Y., 1962, p. 263.

14. E. M. Shoemaker and R. J. Hackman, Interplanetary Correlation of Geologic Time, 7th Annual Meeting, American Astronautical Society, Dallas, Texas, Jan. 1961.

15. A. Lacroix, La Montagne Pelée et ses eruptions, Masson et Cie, Paris, 1904.

16. Robert L. Smith, "Ash Flows", Bulletin of the Geol. Soc. Am. 71, 1960, pp. 795-842.

17. B. N. Moore, "Deposits of Possible Nuée Ardente Origin in the Crater Lake Region, Oregon", Journal of Geology 42, 1934, pp. 358-375.

18. P. O. Rosin and E. Rammler, "Die Kornzusammensetzung des Mahlgutes im Lichte der Wahrscheinlichkeitslehre", Kolloid Zeits. 67, 1934, pp. 16-26.

19. W. C. Krumbein and F. W. Tisdel", Size Distribution of Source Rocks of Sediments" American Journal of Science 238, 1940, pp. 296-305.

20. M. R. Geer and H. F. Yancey, "Expression and Interpretation of the Size Composition of Coal", Inst. Min. and Met. Eng., Tech. Publ 948, 1938.

21. Stephen Brunauer, P. H. Emmett, and Edward Teller, "Adsorption of Gases in Multimolecular Layers", J. Am. Chem. Soc. 60, 1938, pp. 309-319.

22. W. E. Barr and Victor J. Anhorn , Scientific and Industrial Glass Blowing and Laboratory Techniques, Ch. XII Gas Adsorption Apparatus for Measuring Surface Areas, Instruments Publishing Co., Pittsburgh, Pa., 1949, pp. 257-283.

23. M. Leva, "Fixed Bed and Onset of Fluidization" Chapter 3, Fluidization, McGraw-Hill, New York, 1959.

24. G. L. Matheson, W. A. Herbst, and P. H. Holt, II, "Characteristics of Fluid-Solid Systems", Ind. and Eng. Chem., 41, 1949, pp. 1099-1104.